Harnessing icIEF to Unlock Protein-Based Therapeutics

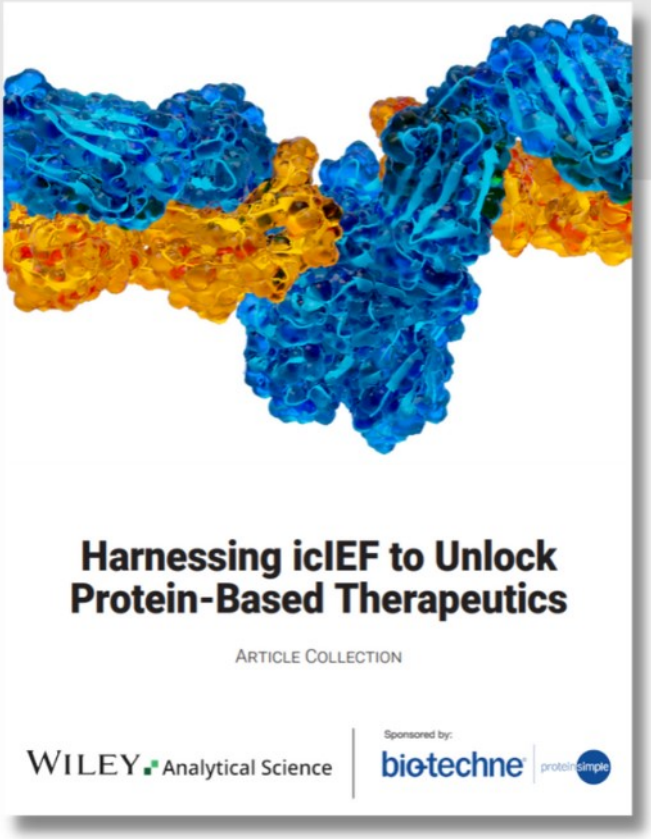

Read the new Article Collection

Keep up to date with the latest developments in biotherapeutics and the range of treatments for various diseases with our latest article collection. Find out how imaged cIEF (icIEF) technique is essential for quality control and analytical development of these drugs, as it accurately determines the surface charge of lipid nanoparticles and the charge heterogeneity of proteins and antibodies.

This article collection aims to provide you with more information on these techniques and technologies, helping you further your research in this field.

bio-techne® | protein simple

WILEY

ADVANCED HEALTHCARE MATERIALS
www.advhealthmat.de

A Novel Patient-Personalized Nanovector Based on Homotypic Recognition and Magnetic Hyperthermia for an Efficient Treatment of Glioblastoma Multiforme

Daniele De Pasquale, Carlotta Pucci,* Andrea Desii, Attilio Marino, Doriana Debellis, Luca Leoncino, Mirko Prato, Stefania Moscato, Simone Amadio, Pietro Fiaschi, Alessandro Prior, and Gianni Ciofani**

Glioblastoma multiforme (GBM) is the deadliest brain tumor, characterized by an extreme genotypic and phenotypic variability, besides a high infiltrative nature in healthy tissues. Apart from very invasive surgical procedures, to date, there are no effective treatments, and life expectancy is very limited. In this work, an innovative therapeutic approach based on lipid-based magnetic nanovectors is proposed, owning a dual therapeutic function: chemotherapy, thanks to an antineoplastic drug (regorafenib) loaded in the core, and localized magnetic hyperthermia, thanks to the presence of iron oxide nanoparticles, remotely activated by an alternating magnetic field. The drug is selected based on ad hoc patient-specific screenings; moreover, the nanovector is decorated with cell membranes derived from patients' cells, aiming at increasing homotypic and personalized targeting. It is demonstrated that this functionalization not only enhances the selectivity of the nanovectors toward patient-derived GBM cells, but also their blood–brain barrier in vitro crossing ability. The localized magnetic hyperthermia induces both thermal and oxidative intracellular stress that lead to lysosomal membrane permeabilization and to the release of proteolytic enzymes into the cytosol. Collected results show that hyperthermia and chemotherapy work in synergy to reduce GBM cell invasion properties, to induce intracellular damage and, eventually, to prompt cellular death.

1. Introduction

Glioblastoma multiforme (GBM) is the most aggressive brain cancer, with an incidence of 2–3 cases per 100 000 people worldwide, accounting for 45.2% of malignant primary brain and central nervous system tumors.[1] Current treatments consist of surgical resection, chemotherapy, and radiotherapy, but the prognosis is still very abysmal. Due to its invasive nature, the complete surgical removal of GBM is almost impossible, with a high recurrence rate (≈90%), and patients often have a limited life expectancy (median survival rate of 12–15 months since diagnosis, five-years survival of ≈5%).[2] The etiological causes of GBM have not been still completely understood; on the other hand, GBM hallmarks are well known. It is, in fact, characterized by an extreme inter- and intratumoral genetic variability, making the selection of a right therapeutic regimen for each patient extremely challenging.[2] Moreover, GBM cells have a high ability to infiltrate healthy brain tissues:[3] this makes the precise location and identification of tumor cells for surgical resection or for targeted treatments extremely difficult. It is known, for instance, that 90% of GBM relapses

D. De Pasquale, C. Pucci, A. Desii, A. Marino, S. Amadio, G. Ciofani
Smart Bio-Interfaces
Istituto Italiano di Tecnologia
Viale Rinaldo Piaggio 34, 56025 Pontedera, Italy
E-mail: daniele.depasquale@iit.it; carlotta.pucci@iit.it; gianni.ciofani@iit.it

The ORCID identification number(s) for the author(s) of this article can be found under https://doi.org/10.1002/adhm.202203120

DOI: 10.1002/adhm.202203120

D. Debellis, L. Leoncino
Electron Microscopy Facility
Istituto Italiano di Tecnologia
Via Morego 30, 16163 Genova, Italy

M. Prato
Materials Characterization Facility
Istituto Italiano di Tecnologia
Via Morego 30, 16163 Genova, Italy

S. Moscato
Department of Clinical and Experimental Medicine
University of Pisa
Via Roma 55, 56126 Pisa, Italy

P. Fiaschi, A. Prior
Department of Neurosurgery
IRCCS Ospedale Policlinico San Martino
Largo Rossana Benzi 10, 16132 Genova, Italy

appear about 1–2 cm from the surgical resection site (the "removal cavity"), in the area named "peritumoral region." GBM is also characterized by the presence of cancer stem cells (CSCs), also known as tumor-initiating cells, that have been related to GBM drug and radiotherapy resistance.[4] Another limitation associated with GBM treatment is the presence of the blood–brain barrier (BBB), a very selective structure that acts as a natural defense against potentially harmful substances that might enter and damage the brain; on the other side, it strongly limits numerous anticancer drugs from reaching the tumor location.[5]

Nowadays, therapies for GBM are scarce, and they are mainly based on the administration of temozolomide in combination with radiotherapy (Stupp protocol),[6] or nitrosoureas-based treatments (carmustine, lomustine, and nimustine).[7] However, the high recurrence rate and the heavy side effects make clear that these strategies are not sufficient to eradicate GBM. In this context, nanotechnology might provide valid options for the systemic delivery of drugs, enhancing their bioavailability and their penetration through the BBB, and, therefore, favoring their accumulation in the tumor with a lower administration dose. Nanoparticles can also act as therapeutic or contrast agents, and they can be easily engineered to be responsive to specific stimuli and/or to target tumor cells.[8] Conventional tumor targeting approaches exploit simple interactions between receptors overexpressed on the target cells and ligands (e.g., antibodies, proteins, peptides, and aptamers) conjugated to the nanoparticles.[8] However, cancer recognition is a multifactorial process that involves the interaction of several membrane proteins.[9] It has been demonstrated that cancer cells are able to recognize each other and form multicellular aggregates through "homotypic affinity," a mechanism mediated by particular membrane proteins in homophilic adhesion domains.[10] By mimicking the natural behavior of cancer cells, a new biomimetic strategy based on homotypic affinity has been developed and can be obtained by coating nanoparticles with cell membranes (CMs) extracted from the target cells.[10] In one of our previous works, we have demonstrated that boron nitride nanotubes coated with cell membranes extracted from U87-MG cells, a common in vitro model for GBM, were able to efficiently target GBM cells in vitro.[11]

In this work, we propose an innovative lipid-based magnetic nanovector exploiting the synergic action of a chemotherapeutic drug and magnetic hyperthermia, and with the ability to target patient-derived GBM cells thanks to the homotypic affinity strategy. In order to achieve this multifunctional goal, the nanovectors are composed of a lipid core containing drug and iron oxide nanoparticles (IONPs), and coated with plasma membrane extracts of patient-derived GBM cells, to obtain cell-derived lipid magnetic nanovectors (CDMNVs). According to this strategy, nanovectors are not only able to be targeted towards GBM, yet they are also tailored to the specific patient's tumor features. Moreover, taking into account the heterogeneity of GBM, a preliminary screening on several known chemotherapeutics allowed us to select regorafenib as the loaded drug basing on the response of the specific patient. Regorafenib (commercialized by Bayer under the name of Stivarga) is a multikinase inhibitor that targets angiogenic, stromal, and oncogenic receptor tyrosine kinases.[12] It has been approved by the Food and Drug Administration (FDA) and by the European Medical Agency (EMA) for the treatment of colorectal cancer, gastrointestinal stromal tumors, and hepatocellular carcinoma,[13,14] while the Italian Medicine Agency (AIFA) has approved regorafenib for the treatment of relapsed glioblastoma,[15] following the encouraging results of the REGOMA trial.[16–18]

We used complex 2D and 3D in vitro models based on patient-derived GBM cells to demonstrate the efficacy of the homotypic targeting and to elucidate the mechanisms of action of the proposed nanovector on a system that closely mimic the real in vivo GBM features. Thanks to the cell membrane coating, the nanovectors are able to selectively target patient-derived GBM cells and to efficiently cross a fluidic BBB in vitro model; our results clearly highlight the pivotal role played by membrane proteins in addressing these two tasks. Magnetic hyperthermia generated by the interaction between IONPs and alternating magnetic fields (AMF) induces thermal and oxidative intracellular stress, triggers lysosomal membrane permeabilization (LMP, one of the mechanisms involved in the cytoxicity of IONPs-induced magnetic hyperthermia[19]) with the release of the proteolytic enzyme cathepsin D into the cytosol, and activates caspase-8-dependent extrinsic apoptotic pathways. Our results suggest that magnetic hyperthermia ensures a wider spectrum of antitumor action and works in synergy with the drug, enhancing the therapeutic efficacy and potentially overcoming issues related to GBM intra- and intertumoral heterogeneity.[19,20]

2. Results and Discussion

2.1. Nanovector Characterization

IONPs synthetized in this work have a mean diameter of 24.4 ± 0.4 nm with a good monodispersity, as shown in transmission electron microscopy (TEM) images in Figure S2A–C (Supporting Information). The crystalline structure, determined by selected area electron diffraction (SAED) profile, is compatible with magnetite (Figure S2D,E, Supporting Information). Thermogravimetric analysis (TGA) shows that the organic component in IONPs, due to the final oleic acid coating, is about 5.5% of the total weight (Figure S3, Supporting Information).

IONPs were then integrated in the lipid formulation to obtain CDMNVs. As shown in **Figure 1**A,B, lipid nanovectors before the coating (MNVs) have a homogeneous size distribution, with an average hydrodynamic diameter and polydispersity index of 240 ± 14 nm and 0.15 ± 0.05, respectively, and a negative ζ-potential of −26.1 ± 0.7 mV. In Figure 1C and Figure S3A (Supporting Information), representative TEM images of MNVs show that IONPs are encapsulated in the lipid matrix and they confer a spherical, blackberry-like structure to the whole nanovector. MNVs were, then, coated with cell membrane extracts, isolated and purified from patient-derived GBM cells to obtain CDMNVs. The size, polydispersity, and ζ-potential of CDMNVs are, respectively, 288 ± 1 nm, 0.17 ± 0.01, and −23.6 ± 0.4 mV, and the size distribution (Figure 1A) is similar to that one of MNVs,

P. Fiaschi
Department of Neuroscience, Rehabilitation, Ophthalmology, Genetics, Maternal and Child Health (DiNOGMI)
University of Genova
Largo Paolo Daneo 3, 16132 Genova, Italy

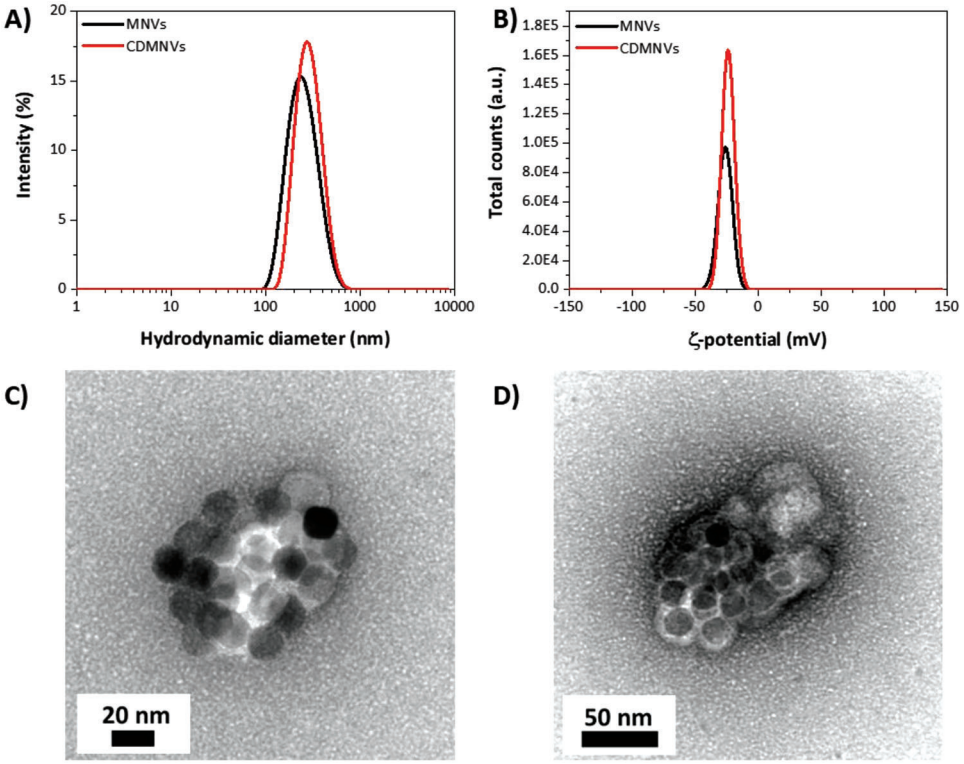

Figure 1. A) Intensity distribution (%) as a function of the hydrodynamic diameter (nm) for MNVs (black) and CDMNVs (red). B) ζ-potential (mV) distribution of MNVs (black) and CDMNVs (red). C,D) Representative BF-TEM images of MNVs and CDMNVs.

suggesting that the coating represents only a small layer around the nanoparticles and does not affect their morphology and stability. The TEM images in Figure 1D and Figure S3B (Supporting Information) confirm the dynamic light scattering (DLS) measurements, since no significant variations in the nanovector morphology could be detected after the coating with cell membrane extracts.

The content of IONPs in both MNVs and CDMNVs was first determined with the colorimetric iron assay; the weight percentage of IONPs with respect to the total nanovectors weight was found to be 77 wt% in MNVs and 67 wt% in CDMNVs (the total weight of the nanovectors was determined by freeze-drying; see the Experimental Section). The increase of the organic component in CDMNVs (+ 10 wt%) with respect to MNVs is consistent with the formation of the coating. TGA results confirm the iron assay; in fact, in this case, IONPs in the nanovectors represent 78.5 ± 0.7 wt% of MNVs and 70 ± 2 wt% of CDMNVs (Figure S4, Supporting Information). Moreover, an increase in the organic component in CDMNVs of about 8.5 wt% is evidenced also by TGA: again, this can be attributed to the formation of a coating. Therefore, by averaging TGA and iron assay results, it can be assumed that the coating with cell membrane extract on CDMNVs represent ≈9 wt% of the total nanovector weight.

A schematic sketch of the coating on the nanovectors is shown in **Figure 2**A. The presence of the cell membrane coating in CDMNVs was characterized by Fourier-transformed infrared (FTIR) spectroscopy (Figure 2B). In MNVs (black curve), CM extracts (blue curve), and CDMNVs (red curve), the P–O stretching due to phospholipids (≈1000–1200 cm^{-1}, light blue box in Figure 2B) and the peaks due to lipid hydrocarbon chain vibrations (CH_2 and CH_2, 3000–2800 cm^{-1}, light red box in Figure 2B) can be found; the presence of the P–O can be observed also in MNVs, before the coating procedure, due to phospholipids, in particular 1,2-dipalmitoyl-*rac*-glycero-3-phosphocholine (DPPC), constituting the lipid core of the nanoparticles. In both MNVs and CDMNVs, a peak corresponding to Fe–O vibrations of IONPs can be detected at around 580 cm^{-1} (light green box in Figure 2B). CM extract and CDMNV spectra show the typical contributions of amide bonds (light purple box in Figure 2B) at ≈1650 cm^{-1} (C=O stretching vibrations) and ≈1540 cm^{-1} (N–H bending and C–N stretching), that are usually found in proteins.[11] Although these signals are low in CDMNVs (highlighted with arrows in Figure 2B) due to a lower amount of proteins in the nanovectors, their appearance is still visible and confirms the successful coating with CM extracts.

To further investigate the cell membrane coating in CDMNVs, X-ray photoelectron spectroscopy (XPS) has been carried out. Figure 2C and Figure S5 (Supporting Information) show that in both MNVs and CDMNVs, the oxidation state of Fe is composed of a mixture of +2 and +3, as expected in Fe_3O_4. By deconvoluting the $Fe2p_{3/2}$ peak, centered at 710.7 eV, and taking into account the contributions of Fe^{3+} (≈713 eV) and Fe^{2+} (≈710 eV) as reported in Hallam et al.,[21] the fraction of Fe^{3+} in IONPs is estimated to be 0.64 and 0.68 in MNVs and CDMNVs, respectively. Considering the explicit stoichiometry $FeO \bullet Fe_2O_3$ for Fe_3O_4, the theoretical fraction of Fe^{3+} in magnetite should be 0.66; therefore, the Fe^{3+}/Fe^{2+} in our IONPs is in line with the typical magnetite stoichiometry, confirming the results obtained with SAED

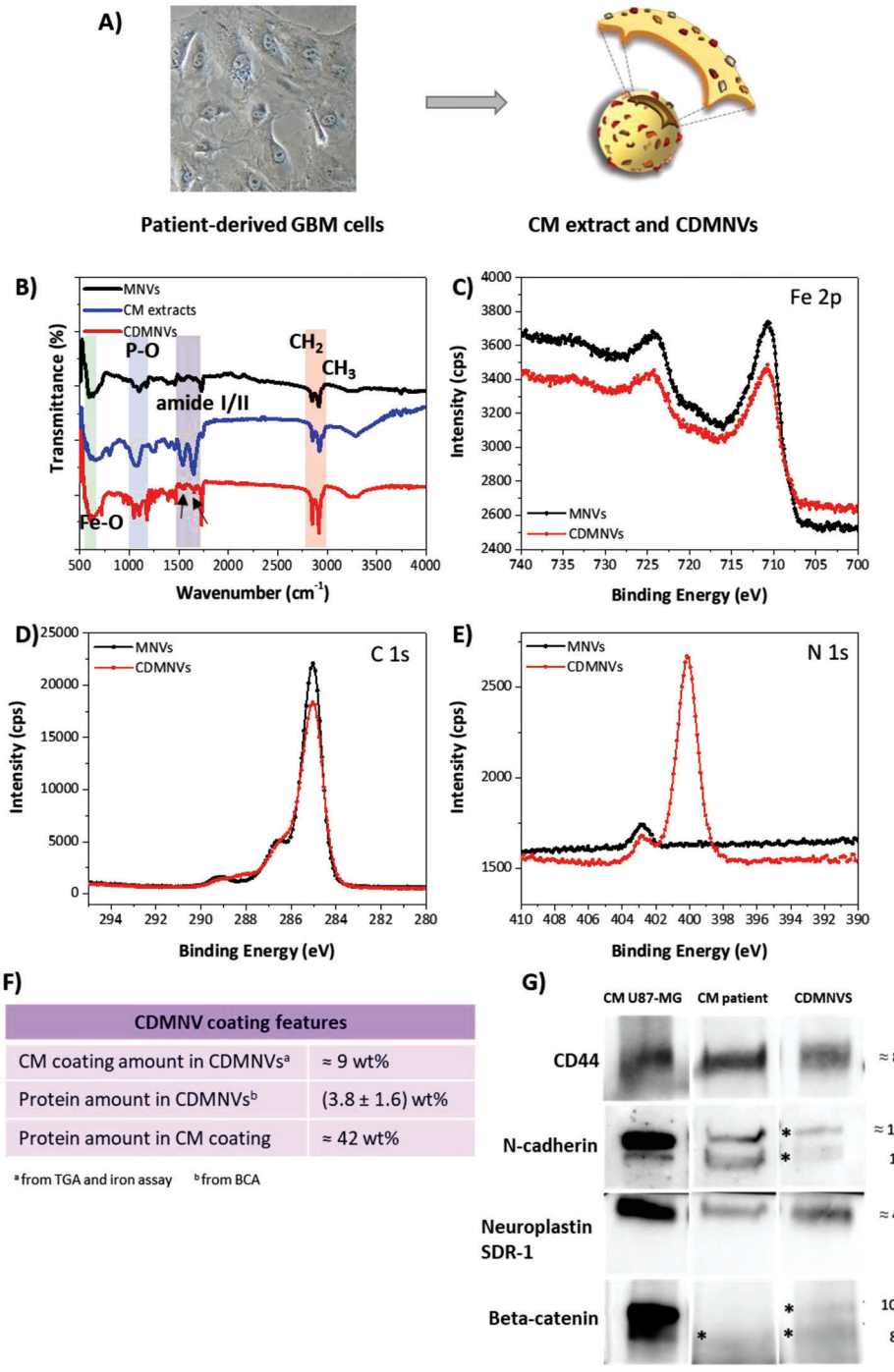

CDMNV coating features	
CM coating amount in CDMNVs[a]	≈ 9 wt%
Protein amount in CDMNVs[b]	(3.8 ± 1.6) wt%
Protein amount in CM coating	≈ 42 wt%

[a] from TGA and iron assay [b] from BCA

Figure 2. A) Scheme of CDMNV coating, with an optical microscopy image of a typical patient-derived GBM cell culture. B) FTIR spectra of MNVs (black), CM extracts (blue), and CDMNVs (red). C–E) High-resolution XPS scans for MNVs (black) and CDMNVs (red) for Fe 2p, C1s, and N1s. F) Table summarizing the feature of the CM coating in CDMNVs. G) Western blotting of typical proteins involved in the homotypic adhesion mechanism (CD44, N-cadherin, neuroplastin SDR-1, beta-catenin) in CM extracts of U87-MG cells and of patient-derived GBM cells and in CDMNVs coated with the CM extract obtained from the same patient's cells; the molecular weight of the proteins is reported on the right.

in Figure S2E (Supporting Information). As a further confirmation, the absence of a satellite peak at 719 eV is also typical of magnetite; peak that is, instead, found in maghemite.[22,23] The signal of C (Figure 2D) has several components: the main one, located at 285 eV, is related to C–C– and C–H bonds; the component at around 286.5 eV is typically assigned to C–OH or C–O–C bonds; in MNVs, a component at around 289 eV, due to –COOH groups, results evident; in CDMNVs, a peak at around 288 eV is also present, that might be due to COO– groups.[24] From the intensity of Fe and C signals, it can be derived that the Fe/C ratio

goes from 2.3% in MNVs to 1.2% in CDMNVs, in agreement with the increase of the organic material in CDMNVs after the coating. Finally, N signal (Figure 2E) in MNVs has only one peak at 402.8 eV due to DPPC, while in CDMNVs there is another intense contribution at 400.1 eV, typical for amines and amides, confirming the presence of the coating.[25] It is worth noticing that the DPPC contribution in CDMNVs is still evident: this suggests that the cell membrane coating is thin (≈10 nm or less); as cell membranes are reported to have a thickness of ≈7.5–10 nm, this finding is therefore in agreement with the formation of a single cell membrane bilayer coating in CDMNVs.[26,27]

Proteins on the cell membrane-derived coating in CDMNVs were quantified, with the BCA assay, to be the 3.8 ± 1.6 wt% of the total nanovector mass. On the other hand, CD*MNVs (i.e., nanovectors coated with deproteinated cell membrane extracts; see the Experimental Section) tested with the same assay gave rise to a very low absorption signal that, if considered reliable, could be translated into a final protein content of 0.6 ± 0.2 wt%. Nevertheless, the intensity was below the detection limit and, therefore, the protein content, if any, can be considered negligible, confirming the efficient protein removal with the procedure used in this work: CD*MNVs can be thus used as a reliable control to highlight the role of membrane protein in nanovector uptake and BBB crossing.

By combining the BCA results on protein content in CDMNVs with those obtained from TGA and the iron assay concerning the amount of the cell membrane coating on CDMNVs, the protein content in the cell membrane extract wrapped around the nanovectors is estimated to be ≈42 wt% of the coating, in agreement with our previous work.[11] Interestingly, it has been previously reported that membrane proteins represent ≈50 wt% of human plasma membranes,[28] a value that is very close to that one found in our CDMNV coating. This suggests that the cell membrane extraction protocol and the nanovector coating procedure can guarantee the preservation of the native structure of plasma membrane, without loss of significant proteins that could be fundamental in the homotypic adhesion mechanism. A table in Figure 2F summarizes the findings obtained by both the iron assay and BCA.

The presence of proteins on the cell membrane coating plays a crucial role in the homotypic targeting process, as they mediate cancer cell recognition. Nevertheless, as we have demonstrated in our previous work, some membrane proteins seem to have a more direct role in this process.[11] Among them, we identified CD44, N-cadherin, neuroplastin-1, and beta-catenin as potential targets in the homotypic affinity mechanism. CD44 is a transmembrane glycoprotein the functions of which mainly concern cell-cell interactions and cellular adhesion, aggregation, and migration.[29] It has been recently demonstrated that CD44 *trans*-homophilic interactions mediate tumor cell aggregation.[30,31] Moreover, CD44 is highly overexpressed in different tumors, including brain tumors, and, for this reason, is often targeted for glioblastoma treatment.[32] N-cadherin is a member of the cadherin superfamily and it is highly expressed in mesenchymal cells and in neural tissues. It plays an important role in calcium-dependent cell-cell adhesion, cell motility, and migration.[33] Neuroplastin has been shown to mediate homophilic interactions by promoting cell adhesion.[34] Beta-catenin has a dual function: it is a pivotal component of the cadherin-mediated cell–cell adhesion complexes and it is also involved in the regulation of gene transcription (Wnt signaling pathway). The presence of these proteins in CM extracts from patient-derived GBM cells and CDMNVs was monitored by Western blotting. A cell membrane extract from U87-MG cells, a common in vitro model for GBM, was used as a positive control, since the presence of these proteins in these cells has been already demonstrated.[11] As shown in Figure 2G (and Figure S6, Supporting Information), both CM and CDMNVs retain all of the four proteins investigated here. This suggests that the extraction and the following coating procedure are successful in maintaining CM functionality and, therefore, CDMNVs can be potentially used to target patient-derived GBM cells through homotypic affinity mediated by cell membrane proteins.

The magnetic properties of IONPs and CDMNVs were evaluated by vibrating sample magnetometry (VSM). The hysteresis loops measured at room temperature (**Figure 3**A) show that free IONPs have a saturation magnetization (M_s) of 39.5 emu g^{-1}, while IONPs encapsulated in CDMNVs show an M_s of 19.2 emu g^{-1}. The M_s of IONPs is lower than that of bulk magnetite (≈90 emu g^{-1});[35] this is common when the crystal is confined in nanometric particles due to surface effects.[36] When IONPs are encapsulated in CDMNVs, there is a further decrease of M_s. As reported in the literature, the presence of a nonmagnetic coating can decrease M_s of IONPs.[37–40] Both free and encapsulated IONPs have a similar coercivity, equal to 33 and 28 Oe, respectively; this value, different from zero, indicates that IONPs do not behave as superparamagnets, and a small remanent magnetization is observed even when the applied field is zero. Nevertheless, the value obtained is consistent with IONPs with a diameter of ≈20 nm.[41,42]

To understand the ability of the nanovectors to induce magnetic hyperthermia when stimulated with an AMF, the temperature of a CDMNV dispersion in water was followed over time during AMF stimulation (frequency $f = 97.55$ kHz; field strength $H = 20$ mT). The selected AMF parameters give rise to an $H \times f$ equal to 1.5×10^9 A m^{-1} s^{-1}, which is threefold higher than the Brezovich limit (≈5×10^8 A m^{-1} s^{-1}), conventionally indicated as the safe $H \times f$ threshold in order to avoid negative effects on patients due to the formation of eddy currents.[19] Nevertheless, more recent in vivo studies have demonstrated that the tolerance level could be increased up to ten times without significant side effects.[43–45] Therefore, the parameters chosen in our study are within these new proposed safety thresholds. As it can be seen from Figure 3B, CDMNVs are able to increase the temperature of the solution from 24.4 °C to almost 32 °C in 30 min. The specific absorption rate (SAR) and intrinsic loss power (ILP) of CDMNVs were calculated from the curve in Figure 3B and normalized to the Fe_3O_4 total mass in the sample. In particular, CDMNVs have a SAR of 14 W g^{-1} and an ILP of 0.57 H m^2 kg^{-1}. These values are in good agreement with those ones found for the free IONPs (SAR = 18.1 W g^{-1} and ILP = 0.68 H m^2 kg^{-1}, measured in hexane, Figure S7, Supporting Information): the encapsulation in the lipid matrix does not therefore significantly affect the magnetic properties of the IONPs; the slight decrease in SAR in CDMNVs might be attributed to an increase of viscosity experienced by IONPs in the lipid matrix.[46]

The stability over the time of CDMNVs in terms of hydrodynamic diameter was evaluated in different conditions (Figure S8, Supporting Information), and namely in water (storage

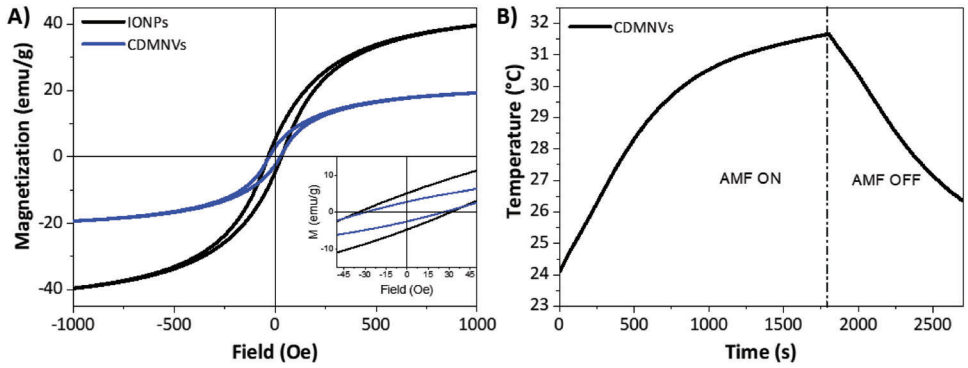

Figure 3. A) VSM measurements for IONPs (black) and CDMNVs (blue) powders acquired at room temperature. Inset: a zoom of the low magnetization and low field area. B) Temperature profile of CDMNVs (3 mg mL^{-1} in terms of iron oxide) during the stimulation with an AMF (AMF ON) and thereafter (AMF OFF).

conditions), at pH 7.4 (DPBS) to mimic the physiological pH, at pH 4.5 to mimic the more acidic tumor microenvironment and/or acidic intracellular organelles (e.g., lysosomes), and in DMEM + 10% FBS to mimic physiological conditions. The last three conditions were also studied adding 100×10^{-6} M H_2O_2, to simulate a physiological environment experiencing oxidative stress, a hallmark of the tumor microenvironment.[47] As depicted by Figure S8 (Supporting Information), the hydrodynamic diameter does not change over the time with the exception of solutions at pH 4.5 (red circles and green diamonds), suggesting that CDMNVs do not have long-term stability in these conditions. Nevertheless, it is worth noticing that in DMEM + 10% FBS, the buffer that more closely mimics the physiological conditions, CDMNVs are stable until 20 days, either with or without the presence of H_2O_2. This is probably due to the formation of a protein corona that further stabilizes the nanoparticles from aggregation and coalescence phenomena. This all considered, CDMNVs can be safely stored in water for long term (at least one month), while their administration to cells guarantees a sufficient stability, well within the time window used to perform the AMF chronic treatment (until 96 h).

2.2. Primary Cell Cultures and Drug Screening

The method of isolation and culturing of primary cells derived from GBM resected tissues provided good outcome in terms of generation of primary GBM cultures with extensive cell viability. The culturing process started from resected tissues provided by the hospital: a representative sample stained with hematoxylin and eosin is shown in Figure S9 (Supporting Information), depicting neoplastic tissue and disorganization of the brain parenchyma typical of GBM, confirming the malignancy of the specimen.

In the context of personalized medicine, we evaluated the patient-dependent response to five different drugs owning known antitumor action. This allowed choosing the best anticancer compound to be loaded in the nanovector among carmustine, nutlin-3a, temozolomide, regorafenib, and sorafenib. Carmustine is a nonspecific alkylating agent that induces crosslinking of DNA and RNA, but it can also bind to and modify glutathione reductase, leading to tumor cell death.[48] It is used against several kinds of brain tumors, and, in particular, it has been approved by the FDA to treat GBM, both by intravenous administration[49] or within a biodegradable wafer implanted during surgery in the resection cavity (Gliadel).[50] Nutlin-3a is a nongenotoxic drug that works as an antagonist of the murine double minute-2 (MDM2) protein, in its interaction with the tumor suppressor protein p53; the inhibition of the MDM2-p53 plays an important role in the reactivation of the p53 pathway and, therefore, in the induction of cell death.[51] In this sense, nutlin-3a has proved to be very effective against p53 wild-type GBM types (e.g., U87-MG cells), with lower efficacy against cells with TP53 mutations.[52,53] Temozolomide is the current standard of care for GBM, usually combined with radiotherapy, following the so-called Stupp protocol.[48] Temozolomide is a prodrug; after hydrolysis and further reactions, the obtained reactive methyl diazonium cation acts as a nonspecific alkylating agent causing a mismatch repair in DNA by methylation at the N-7 or O-6 position of guanine.[54] Nevertheless, several studies have shown a natural temozolomide-resistance (linked to the expression of DNA alkylating proteins and repair enzymes) in some kind of GBM cells, or acquired after treatment.[54] As already mentioned in the introduction, regorafenib inhibits several kind of kinases that are involved in angiogenesis, tumor growth, and tumor microenvironmental signaling pathways.[12] Moreover, it has also been shown to inhibit metastasis in colon cancer.[55] Recently, a phase II clinical trial (REGOMA, NCT02926222) demonstrated regorafenib efficacy in increasing the median overall survival on patients with histologically confirmed relapsed glioblastoma, with respect to the administration of lomustine, another drug of the nitrosourea group.[16] Similarly to regorafenib, sorafenib is a multikinase inhibitor, including VEGFR, PDGFR, and RAF kinases.[56] It has been approved by the FDA for the treatment of unresectable hepatocellular carcinoma, advanced renal cell carcinoma, and metastatic thyroid cancer.[57] Indeed, regorafenib has been obtained as an improvement of the sorafenib molecule, and it differs from the latter just by the addition of a fluorine atom in the center phenyl ring;[12] this slight different chemical structure leads to a different biochemical profile and a higher pharmacological action.[12]

The GBM primary cells response to different concentrations of the above-described drugs was assessed by the WST-1 assay, based on the cleavage of tetrazolium salt to formazan dye by

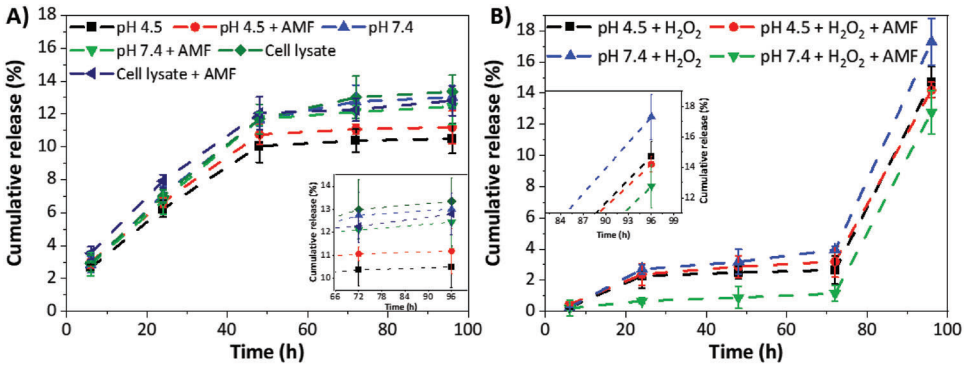

Figure 4. Cumulative release (%) of regorafenib from CDMNVs in different conditions: A) pH 4.5 (black squares), pH 4.5 + AMF (red circles), pH 7.4 (blue triangles), pH 7.4 + AMF (green upside down triangles), cell lysate (dark green diamond), cell lysate + AMF (dark blue left triangles). B) pH 4.5 + 100×10^{-6} M H_2O_2 (black squares), pH 4.5 + 100×10^{-6} M H_2O_2 + AMF (red circles), pH 7.4 + 100×10^{-6} M H_2O_2 (blue triangles), pH 7.4 + 100×10^{-6} M H_2O_2 + AMF (green upside down triangles). In the insets in (A) and (B), a zoom on the release profiles during the last time points to better highlight differences in regorafenib release in the different conditions.

cellular mitochondrial dehydrogenase, directly proportional to the metabolic activity of the cells. The metabolic activity was evaluated at 24 h (Figure S9, Supporting Information) and 72 h (Figure S10, Supporting Information) on cells derived from five different patients. The results of this screening show that patient-derived GBM cells are in general more sensitive to the drugs after 72 h of incubation with respect to 24 h, and that nutlin-3a, sorafenib, and regorafenib overall affect cell metabolic activity at a higher extent in all the tested cultures. The efficacy of regorafenib and sorafenib was found to be higher and less variable among the five patient-derived GBM cells tested with respect to nutlin-3a, characterized by a more pronounced patient-dependent response at lower concentrations. For this reason, nutlin-3a was not selected for the loading in the nanovectors; conversely, considering that regorafenib shows a wide-range efficacy on different patients, and given the recent clinical findings and approval by the AIFA for the treatment of relapsed GBM, it has been selected as cargo of the nanovectors.

2.3. Drug Loading and Release Studies

Following the drug screening results, CDMNVs were loaded with regorafenib to obtain Reg-CDMNVs. The drug loading, evaluated with high-performance liquid chromatography (HPLC), was found to be 1.7 ± 0.5 wt%. The release profile was investigated in different buffers, as depicted in **Figure 4**A,B. The pH 7.4 and pH 4.5 buffers (with or without 100×10^{-6} M H_2O_2) were used to mimic either the physiological pH (pH 7.4) or the more acidic tumor and/or acidic intracellular organelles microenvironment (pH 4.5). In addition to these two conditions, the release was also studied in a buffer constituted of intracellular content directly extracted from patient-derived GBM cells (indicated as "cell lysate"); this condition should more closely represent the real environment experienced by the nanovectors once they have been internalized by cancer cells. In this case, H_2O_2 was not added, since the pH value and the oxidative stress conditions are naturally provided by the buffer. The release was moreover investigated in the presence of the AMF stimulus, with the same parameters used for cell stimulation: 2 h, 20 mT, and 97.5 kHz, applied every day up to 4 d. As depicted in Figure 4A, in absence of H_2O_2, regorafenib release behavior reflects a typical biphasic profile composed of a first burst release (48 h), followed by a slow diffusion-controlled release.[58] According to this model, the drug located in the outer layers of the nanoparticle is usually quickly released, while the drug located in the core of the nanoparticle is released more slowly through pores and/or onset of nanoparticle degradation and hydration.[58] Regorafenib release was not influenced by the application of the AMF. The highest release was observed in the cell lysate buffer at 96 h (13.4 ± 0.9% and 12.8 ± 1%, in absence and in presence of the AMF, respectively). When H_2O_2 is added to both PBS and pH 4.5 buffer, the release profile changes to a biphasic slow diffusion plus rapid erosion profile.[58] It might be speculated that the presence of H_2O_2 modifies the surface of the nanoparticles and changes the solubility of the drug in the buffers, slowing down the release process, especially in the first stage; nevertheless, after a certain amount of time, the onset of hydration and degradation processes might favor a rapid release of the drug. Also in this situation, the AMF stimulation did not play a critical role in drug release, with the highest cumulative release at 96 h (17.3 ± 1.5% at pH 7.4 + H_2O_2).

2.4. Homotypic Targeting of Patient-Derived GBM Cells

Before studying the antitumor effects induced by the synergic action of drug and hyperthermia, we investigated the targeting capabilities of the nanovectors, favored by the cell membrane coating. In particular, we aimed at understanding the role of the plasma membrane proteins in homotypic recognition. In order to accomplish this aim, we used cell models representative of the brain environment, and namely brain endothelial cells (hCMEC/D3), primary human astrocytes, neuron-like cells (derived from SH-SY5Y upon differentiation), and patient-derived GBM cells (the target of the nanovectors). The experiment was carried out with a home-made dynamic bioreactor (Figure S1A, Supporting Information) already proposed for previous studies,[11,20] where the four cell cultures underwent a treatment with either CDMNVs or CD*MNVs, the latter theoretically voided of homotypic targeting abilities.[11]

The results of the experiment are shown in **Figure 5**. The confocal images depicted in Figure 5A qualitatively show the differential uptake of CDMNVs with respect to CD*MNVs. Among all the cell cultures used in the experiment, an appreciable uptake of CDMNVs is evident mainly in patient-derived GBM cells. The analysis of the nanovector internalization confirms this trend (Figure 5B): after 6 h of perfusion, the nanovector uptake by brain endothelial cells, human primary astrocytes and human neuron-like cells was very low or negligible, and no difference between CD*MNVs and CDMNVs could be detected; on the other hand, a clear uptake by patient-derived GBM cells was observed, with a higher internalization of CDMNVs with respect to CD*MNVs (8.0 ± 1.1% of the cell area was occupied by CD*MNVs while 12.0 ± 2.9% by CDMNVs; $p < 0.05$).

It is important to highlight that the proposed nanoplatform owns two fundamental features for patient-personalized medicine: thanks to the drug screening, we selected the most effective anticancer drug to be loaded in the CDMNVs, while the coating is obtained from cell samples derived from the same patient whom the therapy is directed, making the approach highly specific. The cell membrane coating, moreover, guarantee an excellent "camouflage" and highly selective targeting, features that are essential envisioning future in vivo administration.[59]

2.5. Blood–Brain Barrier Crossing Abilities

One of the major limitations of chemotherapy against GBM is definitely the inability of many drugs to cross the BBB, a physiological/anatomical structure able to selectively regulate the passage of substances in the central nervous system. A strategy to overcome this barrier is the functionalization of the nanovectors with molecules that are recognized as "safe" by the BBB, thus allowing the access of the cargo in brain parenchyma. Overcoming the BBB protection system is not an easy task, however some evidences support the strategy of cell membrane camouflaging as a suitable tool to reach the intended site beyond the BBB.[11]

We in vitro tested the BBB crossing ability of CDMNVs / CD*MNVs to underline the role of membrane proteins, by exploiting an in-house developed dynamic bioreactor able to mimic a neurovascular unit (NVU), as described in the Experimental Section (Figure S1B, Supporting Information). The BBB model showed a trans-endothelial electrical resistance (TEER) of 146 ± 50 Ω cm^2, and a P_{app} and P_e with respect to FITC-dextran 70 kDa of 1.8×10^{-6} and 1.9×10^{-6} cm s^{-1}, respectively, values in line the literature.[60]

The results after 3 h of perfusion show that only 3.0 ± 0.1 µg of CD*MNVs passed through the BBB model, i.e., 5.8-fold less with respect to CDMNVs (17.4 ± 0.4 µg; $p < 0.05$). At the end of the perfusion, the nanovector suspension was replaced with fresh medium, and the BBB model was left in the incubator. The medium in the bottom chamber was collected at both 24 and 48 h, in order to evaluate the residual passage of nanovectors, "released" from the cellular components of the BBB (endothelial cells, astrocytes, and pericytes) in absence of a constant nanovector supply, thus mimicking the dynamic conditions experienced by the BBB after in vivo administration. After 24 h, a residual passage through the BBB of 2.01 ± 0.03 µg of CD*MNVs and of 3.12 ± 0.06 µg of CDMNVs ($p < 0.05$) was observed, in line with a preferential uptake of CDMNVs by the BBB model. Finally, 48 h after the treatment, the final residual release was 0.99 ± 0.05 µg for CD*MNVs and 1.02 ± 0.06 µg for CDMNVs (Figure 5C).

The confocal images acquired on the patient-derived GBM cells placed in the bottom chamber of the BBB model are in line with this result: the cell area occupied by nanovectors was 7.1 ± 1.6% in the case of CD*MNVs treatment, while 18.9 ± 2.7% in the case of CDMNVs (Figure 5D,E).

The collected results show that the proteins present in the plasma membrane are indeed able to also favor the passage of the nanovectors through an in vitro BBB model; at this stage, however, an evaluation about which ones are specifically involved in this phenomenon is rather difficult. This notwithstanding, it has been demonstrated that CD44 is directly involved in the migration through the BBB of neural precursor cells,[61] neural stem cells,[62] and leucocytes,[63] and thus we can speculate a significant role of this protein even in the crossing of CDMNVs.

2.6. Internalization Studies

Two main pathways of CDMNV cellular internalization were investigated: clathrin- and caveolin-mediated endocytosis (**Figure 6**A–C). Results show a time-dependent colocalization between CDMNVs and clathrin-coated vesicles (0.23 ± 0.03 and 0.33 ± 0.06, at 6 and 24 h, respectively). The same trend is observed for caveolae, where at 6 h of incubation with CDMNVs the colocalization is 0.15 ± 0.07, while at 24 h is 0.30 ± 0.04. Nevertheless, these results show that there is no preferential internalization pathway for CDMNVs.

The intracellular fate of CDMNVs was investigated considering their possible co-localization with lysosomes. Three different incubation times were considered, to identify the accumulation kinetics that reflects the entire anticancer treatment carried out by the proposed experimental protocol. As shown by the results in Figure 6D,E, the accumulation of CDMNVs in lysosomes increases along the incubation time; by performing Mader's overlap analysis, co-localization signals of lysosomes and CDMNVs are 0.05 ± 0.01 at 6 h, 0.13 ± 0.03 at 24 h, and 0.35 ± 0.04 at 96 h, representing the latter the last time point of the chronic AMF stimulation.

The localization of CDMNVs in lysosomes is promising for magnetic hyperthermia: in fact, it has been previously observed that IONPs sequestered in the lysosomes can favor the permeabilization of the lysosomal membrane upon AMF stimulation, with consequent release of the aggressive lysosomal content in the cytoplasm.[20]

2.7. Patient-Derived GBM Cells Viability after Treatment with CDMNVs and Reg-CDMNVs

Metabolic activity evaluation on patient-derived GBM spheroids incubated with either plain or regorafenib-loaded nanovectors was carried out after 24 and 72 h of treatment; control by using equivalent concentrations of drug have been performed as well (**Figure 7**A,B). Overall, the spheroids maintain a good metabolic activity both at 24 and at 72 h when treated with free regorafenib, at all the concentrations tested. A moderate toxicity was found

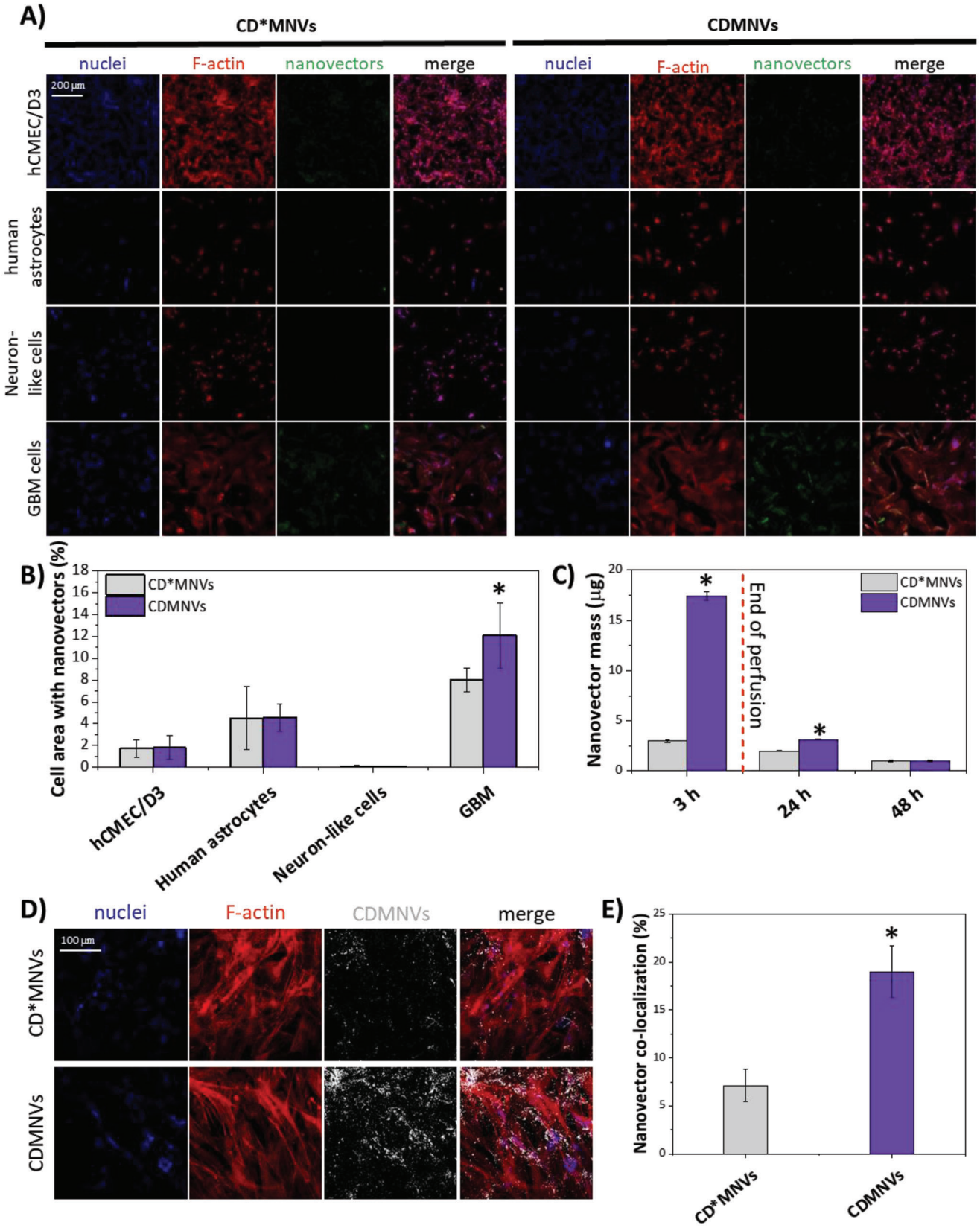

Figure 5. A) Representative confocal images depicting the uptake of CD*MNVs and CDMNVs (in green) by different cell cultures (hCMEC/D3, human astrocytes, neuron-like cells, patient-derived GBM cells) after 6 h of treatment in dynamic conditions. B) Quantitative analysis showing nanovectors/cells

for CDMNVs at 24 h; however, this effect becomes negligible after 72 h. A decrement of metabolic activity upon administration of CDMNVs at high concentrations was expected, since previous studies reported that iron oxide nanoparticles can increase the level of intracellular oxidative stress due to the Fenton reaction associated with iron ions that are released in the lysosomal compartment.[19] Nevertheless, it has been reported that this negative effect on cell proliferation is concentration-dependent and, especially at low concentrations, it has been found to be "transient": treated cells have been in fact shown to recover to values very close to those ones observed in control cells after some time from the administration, when the intracellular concentration of iron oxide is reduced due to cell division.[64,65] Collectively, these results suggest that the plain CDMNVs are not toxic at the tested concentrations, while Reg-CDMNVs show a higher efficacy in reducing metabolic activity of the cells with respect to the plain drug at equivalent concentrations: for example, at 72 h, the metabolic activity of the cells after the treatment with 300 μg mL^{-1} of Reg-CDMNVs (corresponding to 6.8×10^{-6} M of free regorafenib) is $61 \pm 1\%$, conversely it is $109.9 \pm 0.6\%$ after the administration of free 6.8×10^{-6} M regorafenib ($p < 0.05$). This has been already observed in previous works, and it can be explained by considering a more efficient internalization of the drug when encapsulated in nanovectors.[20]

According to the just exposed results, following experiments have been performed by setting the concentration of Reg-CDMNVs at 100 μg mL^{-1}. At these conditions, plain CDMNVs are not toxic, while Reg-CDMNVs show mild effects (yet superior to those ones of the plain drug) that will be presumably amplified by the induction of hyperthermia.

2.8. Effect of Acute AMF Stimulation

2.8.1. Lysosomal Membrane Permeabilization and Release of Proteolytic Enzymes

As mentioned, a possible mechanism of cell death induced by magnetic hyperthermia is mediated by LMP.[19] Magnetic nanoparticles internalized in lysosomes, when stimulated with an AMF, can produce local "hot spots,"[66] inducing severe damage to the lysosomal membrane. Depending on the extent of the damage, the membrane can be permeabilized or completely disrupted, leading to release of the lysosomal cargo and thus to cell death.[67] As a consequence of LMP, the hydrolytic enzymes contained in lysosomes are released into the cytosol. Even though their optimal working pH is the acidic lysosomal pH (4.5–5.0), some of them, like cathepsin B, D, and L, are reported to work with a slower kinetic rate also at the more neutral cytosolic pH; their release can, thus, damage vital cellular components, triggering apoptotic or non-apoptotic cell death pathways.[67] For instance, both cathepsin B and D have been shown to mimic the activity of caspase-8, since they are able to cleave Bid (BH3-interacting domain death agonist), a proapoptotic protein member of the Bcl-2 family; cleaved Bid binds to Bax (Bcl-2 associated X protein) that, in turn, permeabilizes the mitochondrial outer membrane, leading to the release of cytochrome *c*, with consequent activation of caspase-dependent apoptosis.[67,68] Cathepsin B and D can also induce cell death by triggering caspase-independent apoptotic pathways (e.g., through apoptosis-inducing factor translocation from mitochondria to nuclei).[67]

In our previous work, we demonstrated that lipid magnetic nanovectors are successful in inducing LMP and favoring the release of cathepsins upon AMF stimulation,[20] however at an $H \times f$ value significantly high (1.2×10^{10} A m^{-1} s^{-1}, ≈10 times higher than the one used here), and thus rather far from the clinical translation. Here, we assessed LMP through the new nanoplatform and within clinically relevant stimulation range. As we can see from **Figure 8**A, just when cells were treated with nanovectors + acute AMF (2 h), a significant decrease of cathepsin D signal occurred, suggesting its diffusion outside the lysosomes.[68] Quantitative estimation of cathepsin D fluorescence signal support a statistically significant dropping when AMF is used in combination with the magnetic nanovectors (Figure 8B), suggesting LMP is occurring.

LMP is particularly important in antitumor therapy, since lysosomes in cancer cells are more susceptible to disruption with respect to lysosomes of healthy cells.[69] This higher sensitivity is probably attributed to different composition and morphology of lysosomes of cancer cells, characterized by larger size and higher concentration of cathepsins.[69] Moreover, a decreased lysosomal membrane stability in cancer cells could be also due to their higher metabolic and ROS generation rates.[69] LMP induction by AMF can be thus an effective strategy in antitumor therapies, as the specific cue needed to trigger LMP is activated "on demand" when an AMF is applied in presence of magnetic nanoparticles, thus potentially avoiding side effects provided by traditional chemotherapy.[68]

2.8.2. Induction of Intracellular Stress: Expression of Heat Shock Proteins

The nanovector proposed in this work is not only a simple drug delivery system with a customizable tumor targeting capacity, yet, as seen from the LMP induction, it also plays an active role in contrasting tumor growth thanks to magnetic hyperthermia, that induces an intracellular heat shock able to trigger several molecular responses.[70] The stimulation with an AMF can induce an extremely high increase in temperature in the close proximity of the magnetic nanoparticle surface, that exponentially decreases with the distance;[71] this local "hot-spot" can, nevertheless, induce a cellular response, and, depending on the extent, induce cell death. Some of the proteins that are usually found upregulated after magnetic hyperthermia belong to the family of heat shock proteins, such as the molecular chaperone 70 kDa heat shock protein (HSP70).[72,73] HSP70 protects proteins from

co-localization (*$p < 0.05$). C) Quantitative analysis showing the amount of CD*MNVs and CDMNVs in the lower chamber of the BBB in vitro model at different experimental points (*$p < 0.05$); the red dashed line indicates the end of the nanovector perfusion. D) Representative confocal images of CD*MNVs and CDMNVs (in white) internalized by patient-derived GBM cells upon BBB model crossing after 48 h, and E) quantitative analysis showing the nanovectors / cells co-localization (*$p < 0.05$).

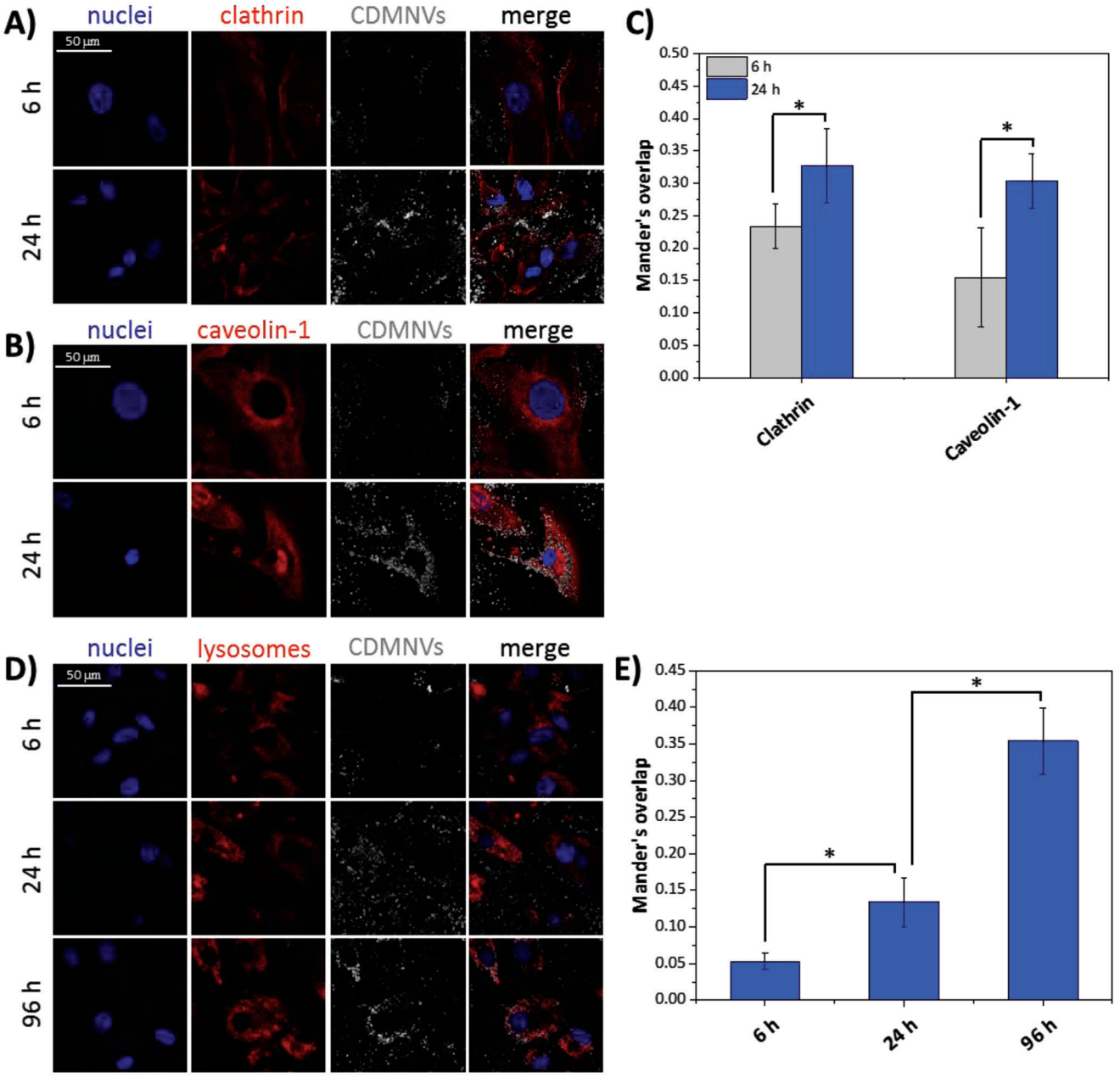

Figure 6. Confocal analysis of the internalization of CDMNVs in patient-derived GBM cells mediated by A) clathrin-coated vesicles or B) caveolae, at 6 and 24 h. C) Quantitative evaluation of colocalization (through Mader's overlap analysis) at 24 and 72 h (*$p < 0.05$). D) Confocal analysis of the co-localization of CDMNVs (in white) with lysosomes (in red) in patient-derived GBM cells after 6, 24, and 72 h of treatment. E) Quantitative evaluation of co-localization through Mader's overlap analysis (*$p < 0.05$).

unfolding during stress conditions, in particular thermal stress, and is active in the cytosol, in the lumen of the endoplasmic reticulum, and in the mitochondrial membranes.[74]

HSP70 is expressed in large quantities when the cell is under hyperthermic stress.[70] Therefore, we investigated the expression of HSP70 in patient-derived GBM cells treated with CDMNVs or Reg-CDMNVs upon AFM stimulation. After acute treatment we observed basal levels of the signal in all the experimental classes (**Figure 9**A,B), but a statistical significant increment when AFM is applied in the presence of magnetic nanovectors (eightfold and threefold higher for CDMNVs and Reg-CDMNVs, respectively; $p < 0.05$). A similar response was also observed in a positive control (cell incubation at 40 °C for the same duration of the acute AMF stimulation). Collectively, these results demonstrate the induction of a significant cellular stress upon the combined AFM + nanoparticles treatment.

Another intracellular stress occurring upon hyperthermia induction is related to the overproduction of reactive oxygen species, in particular at the level of mitochondria. In order to study this effect, we followed the expression of TRAP1, a

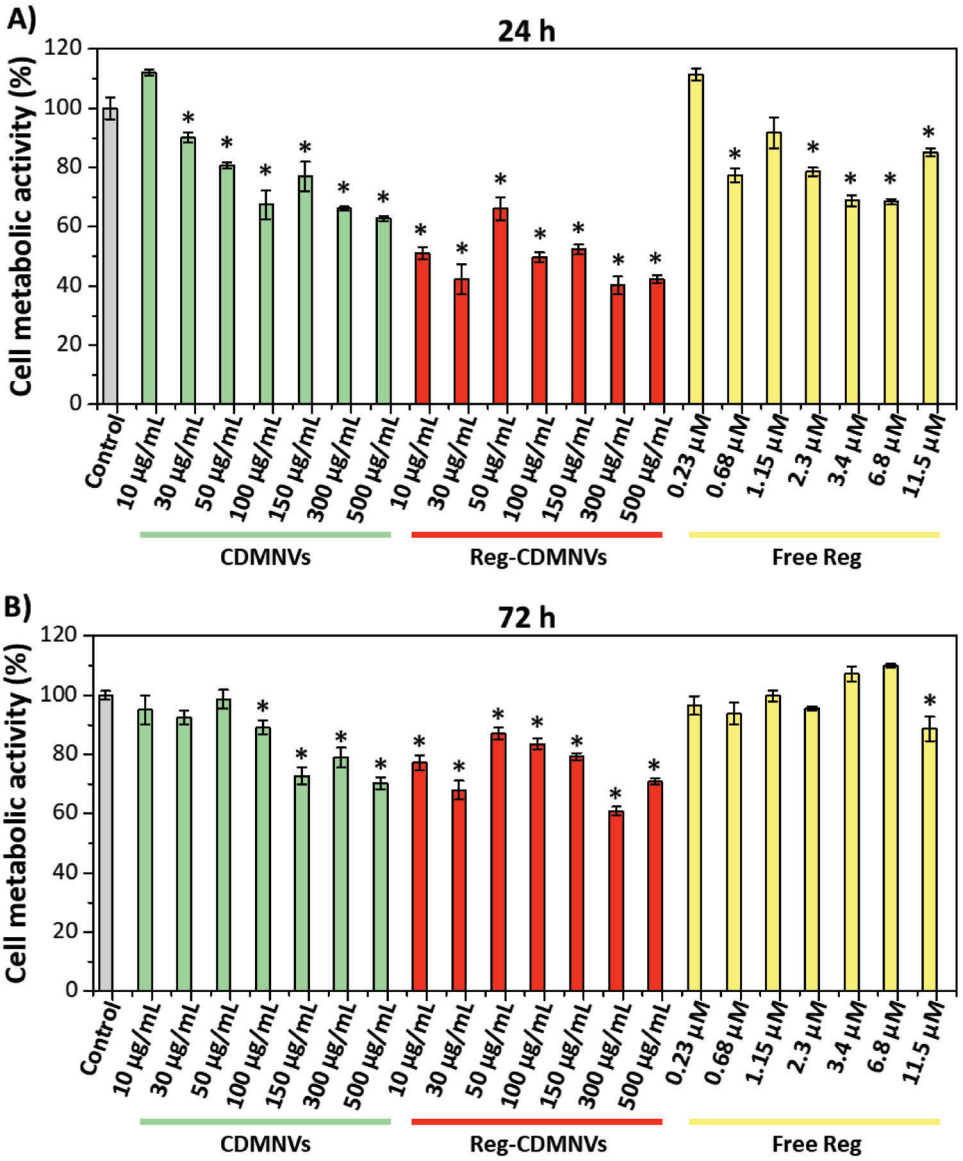

Figure 7. Metabolic activity of patient-derived GBM spheroids treated for A) 24 h and B) 72 h with increasing concentrations of CDMNVs (green), Reg-CDMNVs (red), and free regorafenib (yellow), the latter at concentrations corresponding to the respective loading in Reg-CDMNVs. All data were normalized with respect to control group (gray) (*$p < 0.05$).

chaperone member of the heat shock protein 90 kDa (HSP90) family localized in mitochondria.[75] Several experimental evidences support its crucial role in the regulation of mitochondrial dynamics and in the maintenance of mitochondrial homeostasis under stress conditions, in particular oxidative stress.[75] TRAP1 has in fact be shown to own antioxidant activities, and its expression is upregulated after exposure to oxidative stresses.[76]

In order to monitor the variation of TRAP1 expression in patient-derived GBM cells undergoing the nanovectors + AMF treatment, the same experimental conditions used for HSP70 analysis were followed; in this case, *tert*-butylhydroperoxide (TBH), a commonly used pro-oxidant agent, has been exploited as positive control.

The images in Figure 9C show a higher TRAP1 expression in the CDMNVs + AMF, Reg-CDMNVs + AMF, and TBH-treated experimental groups. The quantitative analysis (Figure 9D) confirm that the upregulation of TRAP1 expression is present just when cells are exposed to the nanovectors (CDMNVs and Reg-CDMNVs) combined with the AMF stimulation (≈ 3-fold and 1.5-fold increment for CDMNVs and Reg-CDMNVs, respectively; $p < 0.05$). Treatment with Reg-CDMNVs without AMF also seems to induce a mild stress at the mitochondrial level (≈2.7-fold; $p < 0.05$), ascribable to the cytotoxic drug delivered inside the cells.

Obtained results suggest that magnetic hyperthermia induces a stress at the mitochondrial level, probably following LMP and the leakage of proteolytic enzymes, that may destabilize mitochondria inducing the permeabilization of their membrane

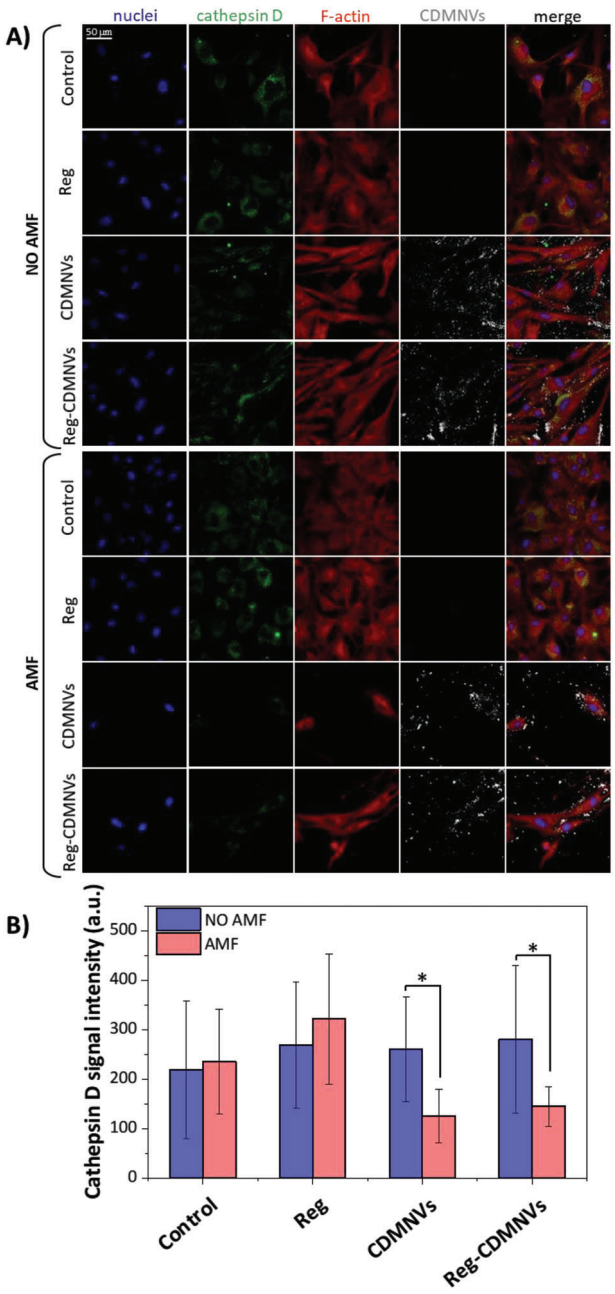

Figure 8. A) Representative cathepsin D confocal imaging (in green) in patient-derived GBM cells after different treatment protocols. B) Quantitative analysis of the cathepsin D signal intensity (*$p < 0.05$).

(mitochondrial outer membrane permeabilization or MOMP) with consequent release of cytochrome *c*.[67] Moreover, an increase of ROS levels in cells treated with IONPs has been already observed in other studies:[77] this is due to a combination of effects, such as the favoring of the Fenton reaction, in which Fe^{3+} and Fe^{2+} catalyze the conversion of hydrogen peroxide (H_2O_2) to hydroxyl or superoxide radicals,[78] to a damage of the mitochondrial membrane,[77] or to the interaction of IONPs with NADPH oxidase in the plasma membrane during internalization.[79] In our study, TRAP1 expression was enhanced after AMF, suggesting a key role of magnetic hyperthermia in favoring ROS production. This was observed, for instance, also by Sola-Leyva et al., that showed how the measured intracellular ROS was high just in cells incubated with magnetic nanoparticles after AMF stimulation.[80] Similar results were also found in other works:[81,82] the increase of the intracellular temperature induced by magnetic hyperthermia might favor ROS production by speeding up the kinetics of the Fenton reaction, by altering cell physiology, or by directly damaging mitochondria.[83,84] It is difficult, at this stage, to identify one of these possible mechanisms as the unique cause of this effect, and, most likely, these results derive from a combination of multiple phenomena.

2.9. Effect of Chronic AMF Stimulation

2.9.1. Migration and Infiltration Capabilities of Patient-Derived GBM Cells

As already discussed, GBM cells have the peculiarity to infiltrate healthy brain tissues, and to generate relapses even far from the initial neoplastic lesion.[85] This ability is provided by the extreme mobility of glioma cells; therefore, the possibility to block the infiltrative property of GBM could represent a tool to hinder possible relapses.

We thus investigated the ability of the proposed treatment protocol to reduce the infiltration and migration capabilities of GBM cells. In **Figure 10**A, bright-field images of patient-derived GBM spheroids exposed to different treatments are presented, while quantitative analyses are reported in Figure 10B. Control spheroids (with or without AMF stimulation) continue to increase their total mass due to cell proliferation, and cells starts to migrate from the surface towards other adhesion sites. In these conditions, the median migration lengths (i.e., the distance travelled by the cells, measured from the edge of the spheroid to the furthest migrated cell) resulted to be 275.4 μm (no AMF) and 263.4 μm (with AMF). A similar behavior is observed also on spheroids treated with free regorafenib (with or without the AMF) and with CDMNVs and Reg-CDMNVs without AMF stimulation, but with the difference of a lower migration length with respect to control spheroids, resulting into a qualitatively reduced volume after 96 h (Figure 10A,B). When the AMF is applied in combination to the nanoparticles, a total hindering of cell motility is observed (−15.8 μm for CDMNVs + AMF and −19.0 μm for Reg-CDMNVs +AMF). The negative values suggest a contraction of the spheroid size at the end of the treatment, suggesting the latter being effective in preventing cell migration and tumor mass increment.

2.9.2. Decrease of Metabolic Activity of Cells during Chronic AMF Stimulation Protocol

In order to describe how the patient-derived GBM cells respond to a chronic stimulation treatment and understand the kinetics of the phenomena, we daily analyzed the metabolic activity of cell after each AMF stimulation (**Figure 11**A). The results show that the control cells maintain a high metabolic activity throughout all the treatment duration, without and with AMF, while the cells

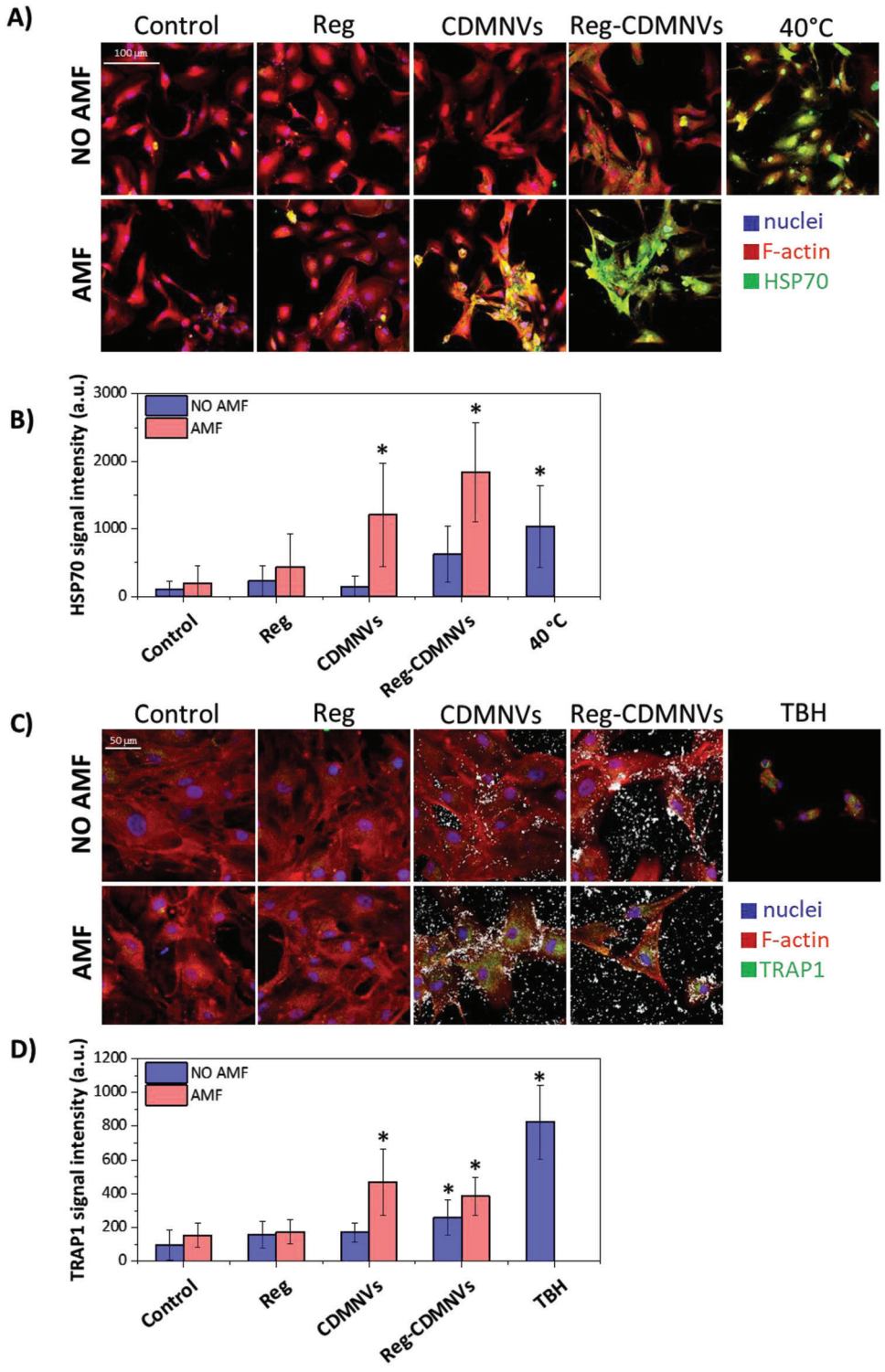

Figure 9. A) Representative HSP70 confocal imaging (in green) in patient-derived GBM cells after different treatment protocols. B) Quantitative analysis of HSP70 signal intensity (*$p < 0.05$). C) Representative TRAP1 confocal imaging (in green) in patient-derived GBM cells after different treatment protocols. D) Quantitative analysis of TRAP1 signal intensity (*$p < 0.05$).

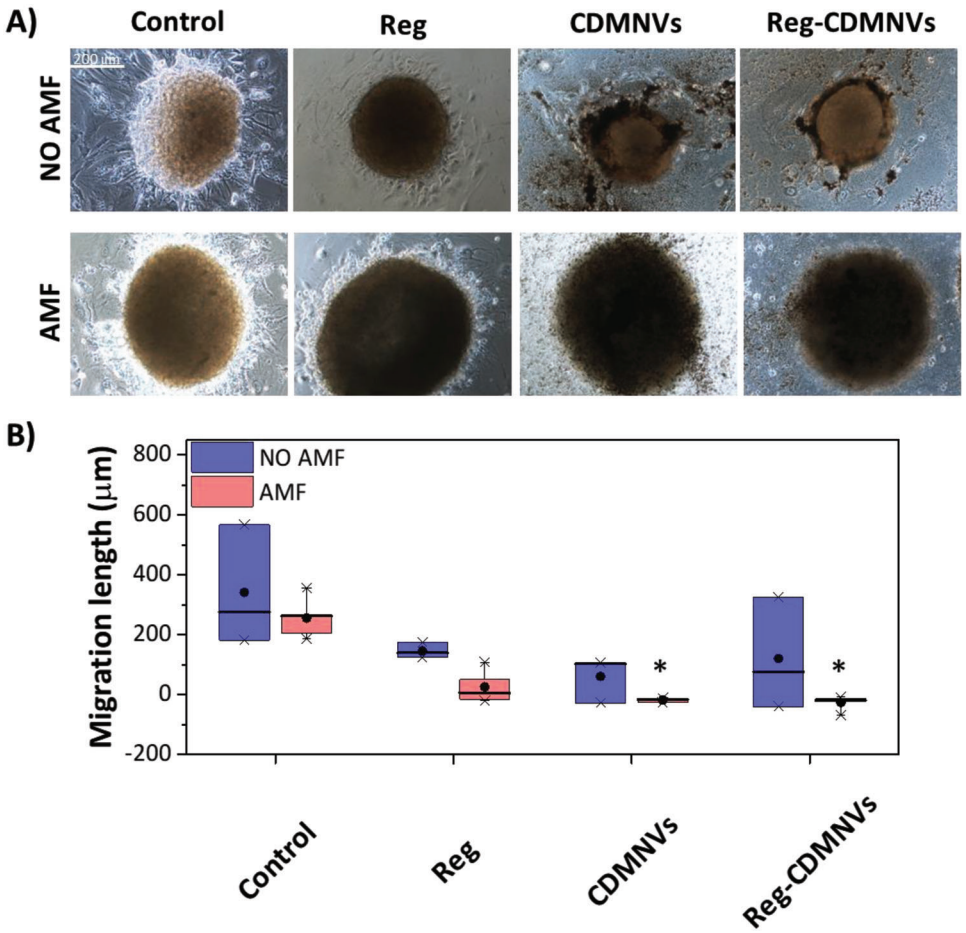

Figure 10. A) Representative optical images of migration tests performed on patient-derived GBM spheroids treated with different experimental protocol. B) Quantitative analysis of the migration length of cells from patient-derived GBM spheroids represented as box chart. The box represents the interquartile range, the bold line is the median, the circle is the average, the bar is the 5%–95% percentile, and the crosses are the minimum and the maximum value (*$p < 0.05$).

treated with free regorafenib undergo an initial phase where the metabolic activity decreases, but it increases back at the third day of treatment. This can be explained by an increased resistance toward the drug.[86] Considering the high intratumoral heterogeneity of GBM, it might be possible that some of the most sensitive cells are initially suppressed by the action of the drug, leading to an overall decrement of cell metabolic activity; however, after a certain time, cells resistant to the drug continue proliferation. This is an undesired outcome of chemotherapy, because it generates tumors that are insensitive to the drug and gives rise to relapses that are more difficult to treat.

Concerning the treatment with CDMNVs without AMF, cells initially undergo a slight decrement in metabolism, as already shown in the preliminary experiments, but this is quickly reverted to values similar to those ones of control groups. Conversely, cells treated with CDMNVs + AMF show a daily decrease of metabolic activity until reaching 25.0 ± 6.4% at the end of the treatment, with a statistically significant difference with respect to the control groups ($p < 0.05$). The best antitumor effect was observed for the treatment with Reg-CDMNVs in the presence of AMF, at the end of which the minimum metabolic activity values were observed (day 1: 45.5 ± 4.2%, day 2: 27.7 ± 4.1%, day 3: 9.2 ± 4.7%, day 4: 11.9 ± 3.0%). Without the application of AMF, the group treated with Reg-CDMNVs shows an initial decrement of metabolic activity, followed by a recovery analogous to that one observed in the case of treatment with plain drug.

This experiment clearly indicates how the synergic action between drug and magnetic hyperthermia leads to the best therapeutic outcome, being able to overcome drug resistance phenomena by attacking tumor cells at different levels and triggering different intracellular responses (i.e., LMP) and stresses, such as thermal and oxidative stress. Results in Figure 11 also highlight the importance of the chronic stimulation in obtaining a more efficient and radical effect. In any case, these tests have been conducted right after the chronic stimulation protocol, and possible effects linked to cell recovery in the days following the treatment have not been investigated at this stage.

In order to better describe apoptotic phenomena following the chronic stimulation, the activation of caspases was taken into consideration, and specifically caspase-8. Caspase-8 is involved in the extrinsic apoptosis pathway, and it is activated at the cytosolic side of the cell membrane by death receptors (e.g., CD95,

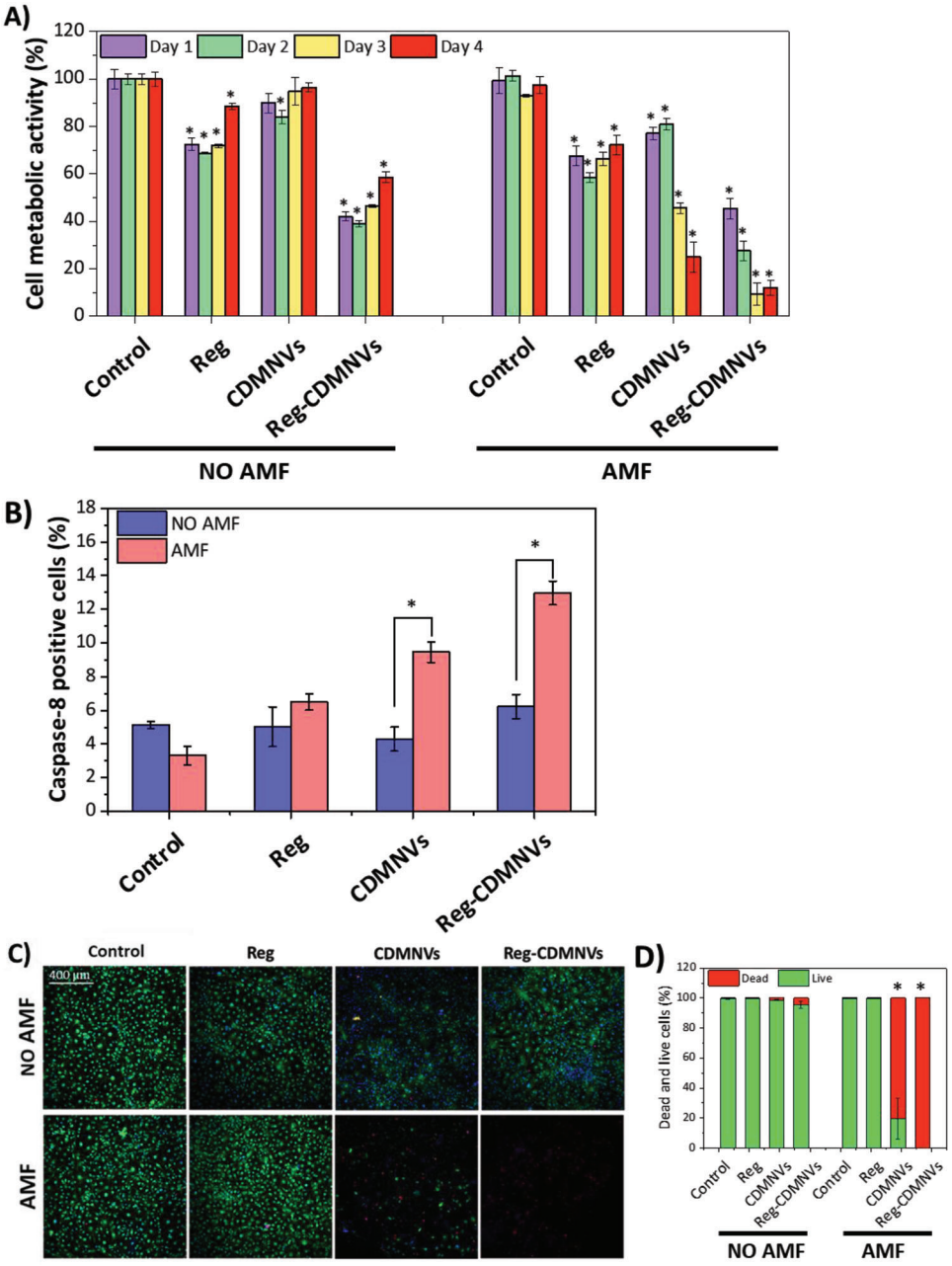

Figure 11. A) Metabolic activity of patient-derived GBM cells upon different treatment protocols. B) Investigation of the expression of caspase-8 in patient-derived GBM spheroids in analogous experimental groups (*$p < 0.05$). C) Representative confocal images of the live/dead assay on patient-derived GBM cells treated with regorafenib, CDMNVs, or Reg-CDMNVs, with or without AMF stimulation. D) Dead and live cells (%) quantified from the analysis of the images in B (*$p < 0.05$).

TRAIL), which are, in turn, activated by specific ligands provided by the environment or by neighboring cells.[87,88] Caspase-8 can directly activate the executioner caspase-3 or caspase-7, thus initiating apoptosis (Type I pathway), or can cleave Bid, activating the intrinsic mitochondrial apoptotic pathway (Type II pathway).[89]

Figure 11B and Figure S11 (Supporting Information) show results obtained on patient-derived GBM spheroids upon the different treatment protocols previously described. Control group and regorafenib-treated group do not exhibit high activation of caspase-8, and similar results were obtained in spheroids treated with CDMNVs and Reg-CDMNVs, without AMF. However, the situation is clearly different when spheroids treated with CDMNVs and Reg-CMNVs undergo the AMF chronic stimulation, with a statistically significant increment of caspase-8 activation (1.8-fold for CDMNVs and 2.5-fold for Reg-CDMNVs, with respect to the control group; $p < 0.05$). Obtained data suggest an activation of the extrinsic apoptotic pathway: an advantageous

strategy since mutations in tumor cells make them more resistant to the induction of the intrinsic pathway.[89]

Our results are in line with what observed by Beola et al.[90] In their work, they demonstrated how the concentration of magnetic nanoparticles internalized by the cells plays an important role in directing cell death towards intrinsic or extrinsic apoptosis. In particular, high levels of intracellular nanoparticles trigger caspase-8 activation, while lower concentrations activate the intrinsic pathway. However, the phenomenon is quite complex and, as the authors stated, it can be affected by other parameters such as cell type, size of the lysosomes giving rise to LMP, or time passed from nanoparticle administration until AMF exposure.[90] The treatment proposed in the present work is able to induce the activation of caspase-8, but it also upregulates proteins (e.g., Hsp70 and TRAP1) associated with intracellular stresses, that can conversely trigger also intrinsic apoptotic pathways. A multimodal attack strategy is thus suggested, particularly useful in case of a heterogeneous pathology like GBM, where a huge intra- and inter-patient response is expected.[2,86]

A final test aiming at evaluating the viability of cells at the end of the stimulation protocol has been performed: the live/dead differential staining (Figure 11C,D) clearly confirm that the cultures subjected to chronic treatment with CDMNVs + AMF or Reg-CDMNVs + AMF have a significant level of necrotic cells (red-stained with ethidium homodimer-1: 80 ± 14% and 100 ± 1% for CDMNVs + AFM and Reg-CDMNVs + AFM, respectively), while other cultures show a high number of viable green-stained (calcein) cells. It is also worth noticing that the free drug and the Reg-CDMNVs without AMF stimulus do not induce a significant cell death (0.2 ± 0.1% and 4 ± 2%, respectively), conversely to the metabolic activity results reported in Figure 11A, suggesting that the drug mainly affects the cell metabolism, rather than inducing an effective apoptosis/necrosis pathway (as also suggested by caspase-8 activation, Figure 11B).

3. Conclusions

Finding an efficient treatment against GBM currently represents an unmet need. Many problems related to this tumor make the challenge even more difficult, such as its genetic heterogeneity, the presence of the BBB, and the problem to efficiently target the treatment to tumor cells to avoid side effects on the healthy tissues. In particular, in GBM, the patient-dependent response to drugs is one of the major challenges that makes the selection of a therapeutic regimen very difficult. In this work, we designed, prepared, and characterized a patient-specific nanovector composed by a lipid core loaded with magnetic nanoparticles and an antineoplastic drug selected from a library according to its efficacy towards a specific patient. The crossing of the BBB and the cancer cell targeting abilities have been obtained via coating of the nanovectors with patient-derived GBM cell membranes, obtained from the patient's cancer specimens, and guaranteeing homotypic cell recognition mediated by specific cell membrane proteins. Even though magnetic hyperthermia in combination with chemotherapeutics is not a completely new strategy, to the best of our knowledge this is the first platform against GBM that proposes such kind of multimodal and patient-personalized nanovector, that not only bears the specific patient's tumor signature on its surface, but it also delivers a drug selected based on the patient's cell response. Owing to the magnetic component, Reg-CDMNVs perform an active action by promoting localized hyperthermia when exposed to an AMF, with parameters very close to those ones recommended for clinical applications. The efficacy of Reg-CDMNVs + AFM was tested on 2D and 3D in vitro models obtained from patient-derived GBM cell cultures, an in vitro model providing a significant improved reliability and predictability with respect to standard cell lines, yet also with respect to in vivo models, often envisioning the use of immune-compromised animals. Obtained results showed a good antitumor activity of the Reg-CDMNVs + AFM protocol, suggesting synergic effect of chemotherapy and magnetic hyperthermia, a strategy that could potentially overcome many problems related to the high variability of GBM. Our work aims at proposing a therapeutic platform that undertakes a comprehensive approach, starting from the extraction of patient-derived material to the "ad hoc" design of the nanovector and its testing on complex in vitro models: the proposed nanoplatform represents the first example of patient-specific and precision nanomedicine against GBM, being based on highly personalized nanoparticles designed and tested through a "patient-centric" approach.

4. Experimental Section

GBM Patient-Derived Cell Cultures: Primary cell cultures of GBM were obtained upon informed written consent from five different patients' resected tissues immediately after surgery, at San Martino Hospital (Genova, Italy), in patients diagnosed with a grade IV primary glioma, IDH-1 wild type, in agreement with procedures approved by the local ethical committee (*Registro CER Liguria* 341/2019).

After surgery, resected tissues were placed in 15 mL tubes filled with sterile physiological solution, and stored at 4 °C until arrival at processing facilities. Subsequently, samples were washed twice with Dulbecco's phosphate buffered saline solution (DPBS, Euroclone) before performing a mechanical separation of the tissue. The resected tissues were placed into a Petri dish (10 cm diameter, Corning), filled with 5 mL of DPBS, and reduced in small pieces with a scalpel. When microscopic pieces were obtained, the supernatant was collected and sieved using 70 µm cut-off sieves (Corning). The filtered cell suspension was cultured in Petri dishes (10 cm diameter) with 10 mL of high-glucose Dulbecco's Modified Eagle's Medium (DMEM, Sigma-Aldrich) with penicillin/streptomycin (Pen/Strep, Euroclone), 1% L-glutamine (Gibco), and 10% fetal bovine serum (FBS, Sigma-Aldrich). From now in advance, this composition will be indicated as "complete DMEM."

After 3 d, the obtained patient-derived GBM cell cultures were washed from the debris with DPBS, and culture medium was replaced with fresh complete DMEM. When cells reached ≈80% confluence, they were washed with DPBS without calcium and magnesium (Euroclone), and then incubated for 7 min with 2 mL of 0.05% trypsin/EDTA solution (Gibco). Afterward, cells were centrifuged at 610 *g* for 5 min and seeded in three different Petri dishes with 10 mL of complete DMEM. After the second passage in culture, the cells were used for the experiments.

Cell Membrane Extraction: GBM patient-derived cells were seeded in 10 cm diameter Petri dishes and, after reaching complete confluence, they were washed twice with DPBS w/o Ca^{2+} and Mg^{2+} (Euroclone) and removed from the dish with a cell scraper (Corning) in 3 mL volume of cold (4 °C) sterile ultrapure water. The cell suspension was immediately placed on ice and injected into a high-pressure homogenizer (Avestin), at a pressure of 20 psi. After three homogenization cycles, the solution was collected and centrifuged at 10 000 *g* for 10 min at 4 °C. The supernatant was collected and centrifuged again with a supercentrifuge (Sorvall Lynx 4000, Thermoscientific) at 37 000 *g* for 60 min at 4 °C in 1.5 mL centrifuge tubes (Beckman coulter). Eventually, the supernatants were removed and the pellets resuspended in a volume of DPBS in order to obtain 1 mL of

suspension from 4.8×10^5 cells, that was thereafter incubated with 5 µL of porcine DNase (Sigma-Aldrich) at 37 °C for 1 h in order to remove DNA residues from the extract. Eventually, a centrifugation step at 37 000 *g* for 60 min at 4 °C was performed to collect the cell membrane pellet, finally resuspended in 1 mL of ultrapure water, to obtain a final purified ready-to-use CM extract.

In order to obtain a suitable "negative" control for the selective targeting experiments, part of the CM extract was processed to remove membrane proteins. The CM pellet was resuspended in DPBS, and 60 µL of porcine proteinase K (1 mg mL^{-1} solution stock of 0.5 U mg^{-1}, Sigma-Aldrich) were added. The suspension was incubated at 37 °C overnight; thereafter, 60 µL of trypsin/EDTA 0.05% were added, and incubated at 37 °C for further 3 h. At the end, the deproteinated CM extracts (now indicated as CM*) were centrifuged at 37 000 *g* for 1 h at 4 °C (Sorvall Lynx 4000,Thermoscientific), and the obtained pellet resuspended in 1 mL of ultrapure water. The removal of proteins was verified by the bicinchoninic acid (BCA) assay (see following sections for details).

IONP Synthesis: IONPs were synthetized from an iron oleate precursor, prepared by reacting 1.8 g of iron (III) chloride ($FeCl_3$, Sigma-Aldrich) with 6.3 g of sodium oleate (TCI) in 10 mL of water, 13.35 mL of ethanol, and 23.35 mL of hexane, under a nitrogen flow.[91] The mixture was heated at 70 °C under reflux and then left at 70 °C for 2 h. After cooling, the organic phase containing the iron oleate was separated from the aqueous phase, and the residual solvents were removed first with a rotavapor, and then under vacuum at 50 °C overnight. To synthetize IONPs from iron oleate thermal decomposition, 6 g of iron oleate were mixed with 25.4 g of eicosane (TCI) and 3.66 mL of oleic acid (Sigma-Aldrich).[91] The reaction was conducted in argon flow, increasing the temperature to 350 °C at a rate of 2 °C min^{-1} under reflux. Once the mixture reached 350 °C, the temperature was kept stable for 30 min. In order to increase the amount of Fe^{3+} in the formed nanoparticles and favor the crystallization into a magnetite phase, a subsequent oxidation step was performed. 1.2 g of trimethyl amine N-oxide (TCI) were added to the freshly formed IONPs and annealed in argon under reflux at 350 °C (heating rate 3 °C min^{-1}, kept at 350 °C for 10 min). Finally, the oxidized IONPs were cleaned by three centrifugation steps in a mixture of chloroform/acetone/methanol at 9960 *g* for 10 min, and eventually redispersed in chloroform to obtain a final concentration of 10 mg mL^{-1}.

Cell Membrane-Coated Lipid-Based Magnetic Nanovectors Formulation: The preparation of the magnetic MNVs was performed by following a procedure optimized from a previous work.[20] Briefly, 17.5 mg of 1-stearoyl-*rac*-glycerol (GMS, Sigma-Aldrich) and 2 mg of DPPC (Sigma-Aldrich) were mixed with 500 µL of a 10 mg mL^{-1} solution of IONPs in chloroform and heated at 70 °C. 3 mL of an aqueous solution (1.0 wt%) of Tween 80 (Sigma-Aldrich), previously heated at 70 °C, were added to the melted lipid/IONPs mixture; the dispersion was then vortexed and sonicated for 10 min (amplitude 90%) with an ultrasonic tip (Fisherbrand Q125 Sonicator). MNVs were cooled down at 4 °C for 30 min and purified by centrifugation (16 000 *g*, 90 min, at 4 °C for three times), and finally redispersed in Milli-Q water (Millipore). Thereafter, MNVs were coated with CM extracted from patient cells to obtain CDMNVs. Around 5 mg of MNVs were mixed with five pellets (deriving from about 2.4×10^6 cells) of CM extracts in 3 mL of sterile Milli-Q water. The dispersion was sonicated with an ultrasonic tip for a total of 20 min at 20% amplitude (in "pulse" mode: 59 s ON, 20 s OFF) in an ice bath to avoid thermal denaturation and defolding of membrane proteins. Thereafter, CDMNVs were purified by three steps of centrifugation (16 000 *g*, 90 min, 4 °C) and finally redispersed in Milli-Q water.

Nanovectors coated with deproteinated cell membrane extracts (CD*MNVs) were prepared following the same procedure. Drug-loaded nanovectors (Reg-CDMNVs) were synthesized by adding and 1 mg of regorafenib (MedChemExpress) to the initial lipid mixture. Nanovectors labeled with fluorescent Vybrant DiO cell-labeling dye (Invitrogen) were analogously prepared, with the addition of 10 µL of dye in the lipid mixture.

The concentrations of the nanovector dispersions were assessed by weighting the dried pellets of known volumes of each dispersion upon freeze-drying.

Characterization of Cell Membrane-Coated Lipid-Based Magnetic Nanovectors: The concentration of iron (Fe) and the relative weight percentage of IONPs encapsulated in the nanovectors was determined at the end of each formulation procedure with a 1,10-phenantroline-based colorimetric assay. 40 µL of a diluted solution of IONPs, MNVs, CDMNVs, Reg-CDMNVs, or CD*MNVs were incubated with 20 µL of hydrochloric acid (37%, Sigma-Aldrich) at room temperature for 4 h. Thereafter, 100 µL of hydroxylamine hydrochloride (100 mg mL^{-1} in water, Sigma-Aldrich) were added to reduce all Fe(III) to Fe(II). The solution was then buffered with 1.8 mL of sodium acetate 500×10^{-3} M (pH 4.5), and 200 µL of a 3 mg mL^{-1} aqueous solution of 1,10-phenantroline (ACROS Organics) were added. 1,10-Phenantroline and Fe(II) form a coordination complex with a pink color, the absorbance of which can be measured at 510 nm with a UV–vis spectrometer (Lambda45 PerkinElmer), and correlated to the Fe concentration in the solution by exploiting a calibration curve. To determine the concentration of iron oxide (magnetite, chemical formula Fe_3O_4) in the IONPs, Fe concentration obtained from the assay was divided by 0.72, which represents the fraction (in weight) of Fe in magnetite. Finally, the percentage in weight (wt%) of IONPs with respect to total mass of the nanovectors was determined with Equation (1)

$$\text{IONPs wt\%} = \frac{m_{\text{IONPs}}}{m_{\text{TOT}}} \cdot 100\% \quad (1)$$

where m_{IONPs} is the mass of IONPs determined by the 1,10-phenantroline-based colorimetric assay and m_{TOT} is the total mass of the nanovectors, obtained by freeze-drying.

IONP size, morphology, and crystalline structure were investigated by TEM-based techniques. A dispersion of IONPs 100 µg mL^{-1} in chloroform was sonicated (2 min, 80 W) and then a drop (≈10 µL) was cast on an ultrathin carbon film on Ni grid. The size and morphology were detected in bright-field TEM imaging mode, while the crystalline phase was studied by SAED technique. Data were acquired using a JEM-1400Plus (JEOL) equipped with a thermionic source (LaB_6, operated at 120 kV) and with a Gatan CCD camera Orius 830 (2048 × 2048 active pixels). The size and morphology of MNVs and CDMNVs were also analyzed by TEM. The samples (100 µg mL^{-1} in water) were sonicated for 2 min and a drop was cast on a Cu grid (150 mesh) coated with an ultrathin amorphous carbon film, and stained with 1% uranyl acetate in water. Images were acquired with a JEM-1011 (JEOL) operated at 100 kV.

TGA was carried out with a Q500 analyzer (TA Instruments) on 4 mg of freeze-dried samples in the temperature range of 30–600 °C, at 10 °C min^{-1}. Cooling was achieved with a 50 mL min^{-1} nitrogen flow.

DLS measurements were performed with a Zetasizer NanoZS90 (Malvern Instruments Ltd.) at 37 °C in order to determine the hydrodynamic diameter of MNVs and CDMNVs. The hydrodynamic diameter and polydispersity index were derived from cumulant analysis of the obtained correlograms, while the intensity distribution was derived through CONTIN analysis. Before the measurement, a diluted dispersion of the nanovectors (100 µg mL^{-1} in ultrapure water) was sonicated for 30 s with a Bandelin ultrasonic probe (8 W). Electrophoretic mobility measurements to obtain nanovector ζ-potential were performed with the same instrument used for DLS measurements. The stability over time (until 35 d) of CDMNVs was evaluated in different conditions: water, pH 4.5 (0.05 M phosphate buffer), pH 7.4 (DPBS), DMEM + 10% FBS, pH 4.5 + H_2O_2 (100×10^{-6} M), pH 7.4 + H_2O_2 (100×10^{-6} M), DMEM + 10% FBS + H_2O_2 (100×10^{-6} M).

FTIR spectroscopy was carried out in order to highlight the characteristic peaks of CDMNVs, in particular those ones related to the presence of the cell membrane on the nanovector surface. FTIR measurements were performed with a Shimadzu Miracle 10 on freeze-dried samples in the range of 500–4000 cm^{-1} with a resolution of 2 cm^{-1}.

XPS was performed on freeze-dried MNVs and CDMNVs with a Kratos Axis Ultra DLD spectrometer, using a monochromatic Al Kα source (15 kV and 20 mA). Wide scans were acquired at an analyzer pass energy of 160 eV, while high-resolution narrow scans were performed at constant pass energy of 20 eV and steps of 0.1 eV. Detection was performed at a take-off angle $\varphi = 0°$ with respect to the surface normal, and the pressure

in the analysis chamber was lower than 7×10^{-9} Torr. Spectra were charge-corrected to the main line of the carbon 1s spectrum (C–C, C–H bonds), set to 285 eV. Spectra were analyzed using the CasaXPS software (version 2.3.24).[92]

The presence and amount of proteins on the CM coating of CDMNVs was determined with the BCA Protein Kit (Thermo Scientific). Briefly, 25 µL of 10 mg mL^{-1} CDMNVs, CD*MNVs, or MNVs (used as control) were mixed with 200 µL of working solution, and incubated at 37 °C for 30 min. Afterward, the absorbance at 560 nm of 90 µL of sample was measured in triplicate with a Victor X3 plate reader (PerkinElmer) and the amount of proteins was determined using a calibration curve made with serial dilutions of a solution of bovine serum albumin (Sigma-Aldrich) in water in the concentration range 0–500 µg mL^{-1}.

The presence of specific proteins in CDMNVs known to be involved in the homotypic adhesion mechanism (CD44, N-cadherin, neuroplastin SDR-1, beta-catenin)[11] was highlighted by Western blotting. A cell membrane pellet or CDMNVs (1 mg) were mixed with 200 µL of RIPA buffer. The solution was sonicated for 30 s with a Bandelin ultrasonic probe (2 W) in ice and then incubated in ice under agitation for 15 min. Afterward, the solutions were centrifuged for 15 min at 14 000 *g* at 14 °C. The supernatant was collected and the concentration of extracted proteins was evaluated by the BCA assay. Due to low concentration, protein samples were precipitated using trichloroacetic acid (TCA, Sigma-Aldrich). Briefly, 1 volume of TCA 20% was added to 1 volume of protein sample and incubated in an ice-bath for 1 h. Then, samples were centrifuged at 15 000 rpm for 20 min at 4 °C, supernatants were removed, and precipitates washed with 0.5 mL of cold acetone and centrifuged as before (15 000 rpm for 20 min at 4 °C). Acetone wash was repeated once again, and then pellets were left at room temperature to remove the solvent. For SDS-PAGE, samples were resuspended in Sample Buffer 1X with 2-mercaptoethanol (2.5% final concentration, Sigma-Aldrich) and 10 µg/lane proteins were separated on a 4%–20% polyacrylamide gel (BioRad) under reducing conditions. Proteins were then transferred to poly(vinylidene fluoride) (PVDF) membrane (Biorad) using the Trans Turbo Blot system (BioRad). After blocking with 5% dry fat milk in a Tris Buffered Solution (TBS) 1× containing Tween 0.1% (T-TBS) for 1 h, membranes were incubated overnight at 4 °C with different primary antibodies diluted in T-TBS as listed below: anti-N-cadherin 1:500 (GeneTex,), anti-CD44 1:1000 (GeneTex), anti-beta-catenin 1:1000 (GeneTex), and anti-neuroplastin SDR-1 1:125 (Abcam). Secondary antibiotic horseradish peroxidase (HRP)-conjugated antibody (BioRad, 1:2000 in 5% dry fat milk in T-TBS, for 1 h incubation) was used and immunocomplexes were detected by chemiluminescence (ECL clarity, BioRad) using a Chemi-Doc XR (BioRad). All reactions were performed at room temperature unless otherwise specified; the Image Lab Software (BioRad) was used to evaluate the molecular weights of the resulting bands.

Magnetic characterization of IONPs and CDMNVs freeze-dried powders was performed at room temperature by a vibrating sample magnetometer (VSM, MicroMag 3900, Princeton Measurements Corp.) applying an external magnetic field ranging from −1000 to +1000 Oe.

The SAR and ILP of IONPs and CDMNVs were evaluated by recording the increase of temperature of a 100 µL solution (3 mg mL^{-1} in iron oxide content) using an OSENSA single channel optic fiber during a stimulation with an AMF. The dispersions were placed in an NMR tube in the center of a 17 turn 56 mm coil of a MagneTherm device (NanoTherics), and stimulated at a frequency of 97.5 kHz and with a field of 20 mT. The temperature was recorded during the first 1800 s of stimulation (AMF ON) and 900 s after the end of the stimulation (AMF OFF) for CDMNVs in water. IONP temperature profile was, instead, measured in hexane for the first 300 s of the AMF application, and then 300 s after switching off the AMF, due to the different features of the dispersing solvent. The obtained curves were analyzed by the "corrected slope model" proposed by Wildeboer et al., using a corrected slope data analysis program made available by the authors (Excel version).[93]

The loading of regorafenib in Reg-CDMNVs was evaluated by HPLC (Shimadzu LC-20AT), with a C-18 column (150 mm × 4.6 mm i.d., 5 µm particle size) and a mobile phase composed of 82.5% acetonitrile (for HPLC, ≥99.9%, Sigma-Aldrich) and 17.5% H_2O (HPLC Plus, Sigma-Aldrich), pumped in isocratic mode (flow rate 1 mL min^{-1}). The peak due to regorafenib was identified with a UV detector at 264 nm at a retention time of 4 min. For the quantification, 1 mg of freeze-dried Reg-CDMNVs dissolved in 400 µL of acetonitrile were heated at 70 °C. Afterward, 100 µL of cold ultrapure water were added and the sample was centrifuged at 16 000 *g* for 90 min at 4 °C. The supernatant was collected and measured with HPLC. The drug loading (%) was calculated using Equation (2)

$$\text{Drug loading } (\%) = \frac{\text{Regorafenib mass in Reg} - \text{CDMNVs (mg)}}{\text{Total mass of Reg} - \text{CDMNVs (mg)}} \cdot 100 \quad (2)$$

In order to evaluate the drug release profile, 1 mg of Reg-CDMNVs were dispersed in 1 mL of six different buffers: pH 7.4 (DPBS) to simulate the physiological environment, pH 7.4 + 100×10^{-6} M H_2O_2 to simulate the physiological environment in the presence of oxidative stress, pH 4.5 (0.05 M phosphate buffer) to simulate the cancer microenvironment, pH 4.5 + 100×10^{-6} M H_2O_2 to simulate the cancer microenvironment in the presence of oxidative stress, and in the cytosolic solution of patient-derived GBM cells (here called "cell lysate") to mimic the drug release when the nanovectors are located in the cytosol of the cells. The latter has been obtained following the same procedure used to extract cell membranes (see previous section), but collecting, in this case, the second supernatant of 4×10^5 cells undergone physical disruption. Reg-CDMNVs, dispersed in each buffer, were left under agitation at 37 °C and, at specific time points (6, 24, 48, 72, and 96 h), were centrifuged at 16 000 *g* for 90 min at 4 °C and the supernatants analyzed by HPLC. The pellets were redispersed in their respective buffers and left under agitation until the following time point. The effect of the AMF on the release of the drug was studied by stimulating Reg-CDMNVs (previously diluted in each of the six already-mentioned buffers) for 2 h with a MagneTherm device (NanoTherics) at an applied magnetic field of 20 mT, using a water-cooled coil of 17 turns and 56 mm inner diameter, and at a frequency of 97.5 kHz, using a similar chronic stimulation protocol exploited for the cell treatment (see the following sections for details).

Drug Screening: In order to study the specific response of GBM patient-derived cells to different antineoplastic drugs, and to choose the best anticancer drug to be exploited in our study, five different compounds were screened: temozolomide (Sigma-Aldrich), nutlin-3a (Sigma-Aldrich), carmustine (Sigma-Aldrich), regorafenib (MedChem Express), and sorafenib (MedChem Express) at concentrations of 0, 5, 10, 50, 80, and 100×10^{-6} M. All stocks solutions were prepared in dimethyl sulfoxide (DMSO, Sigma-Aldrich) at an initial concentration of 4×10^{-3} M, and then diluted in cell culture medium before the test. The toxicity of DMSO alone was also tested at the highest volumes used to dilute the drugs (dilution factors of 1/50 and 1/40 in cell culture medium) in order to discriminate the effect of the drug from possible effects caused by the solvent. The metabolic activity of cells was assessed at 24 and 72 h after the administration of the drugs on GBM cultures derived from five different patients (10^4 cell cm^{-2} 48-well plates, in triplicate for each experimental class). The day after cell seeding, the drugs were administrated to the cells in 400 µL of complete DMEM. After the defined incubation time, cell culture media were replaced with 300 µL of WST-1 (Abcam) solution (dilution 1/20) in complete DMEM without phenol red (Gibco). After 40 min of incubation at 37 °C in 5% CO_2, the supernatant was collected and placed in transparent 96-well plate to read the absorbance at 450 nm with a VictorX3 plate reader (PerkinElmer). The results were analyzed subtracting the blank (WST-1 solution) from the measurements, and reported as percentage (%) with respect to untreated controls (100% cell metabolic activity).

Patient-Derived GBM Spheroids: To obtain patient-derived GBM spheroids, patient-derived GBM cells were grown in a 10 cm Petri dish until 90% of confluence, and then washed with DPBS w/o Ca^{2+} and Mg^{2+} (Euroclone). 2.5 mL of 0.05% trypsin/EDTA solution (Gibco) were added to detach the cells, and after 8 min at 37 °C, the trypsin was blocked with 6 mL of complete DMEM; a cell pellet was obtained following 5 min of centrifugation at 610 *g*. The cells were resuspended and seeded (with 2×10^4 cells in 500 µL of complete DMEM) in 48-well plate, previously coated with 200 µL of 2% agarose gel in ultrapure water. The seeding in

nonadhesive conditions, provided by the agarose coating, induces the cells to form multicellular aggregates, and, finally, to develop a 3D spheroid, considered "ready-to-test" after 5 d.

Nanovector Internalization Assessment: Patient-derived GBM cells obtained from five different patients were exploited to assess the CDMNV uptake behavior. In particular, obtained patient-derived GBM spheroids were treated with 3 mL of a 100 μg mL^{-1} CDMNV dispersion (coated with CM derived from cells of patient #4) for 24 and 72 h. After the incubation, the spheroids were washed tree times with DPBS (Euroclone) and collected in 2 mL tube, with 40 μL of DPBS. Thereafter, they were sonicated in an ultrasonic bath (Branson) for 10 min to favor disruption, and the amount of uptaken iron oxide was assessed through the evaluation of the iron content (please see previous sections for details). Control spheroids (not treated with the nanovectors) were used as a reference to subtract contribution from Fe naturally occurring in cells.

Selective Targeting in Dynamic Conditions: In order to study the selective targeting promoted by the cell membrane functionalization, 100 μg mL^{-1} of CDMNVs were administrated under flow conditions to different cell cultures to mimic the brain environment. hCMEC/D3 (human brain microendothelial cells, Millipore), human primary astrocytes (Alphabioregen), and GBM primary cells were cultured in EndoGRO-VEGF (Millipore), astrocyte growth medium (Alphabioregen), and complete DMEM, respectively. 10^4 cells were seeded on 1 cm^2 round glass coverslip (VWR) 24 h before the experiment. Human neuron-like cells were obtained from SH-SY5Y (ATCC) in differentiation conditions; 10^4 SH-SY5Y were seeded 8 d before the experiment on 1 cm^2 round glass coverslips (VWR) in DMEM F12 (Sigma-Aldrich) supplemented with 1% glutamine (Sigma-Aldrich), 10% FBS (Sigma-Aldrich), and 1% Pen/Strep (Gibco). After 48 h from the seeding, cell differentiation was induced by replacing the culture medium with high-glucose DMEM (Euroclone) supplemented with 1% FBS, 1% glutamine, 1% Pen/Strep, and retinoic acid 10×10^{-6} M; these culture conditions were maintained for 6 d. Three experimental replicates were prepared for each experimental class. On the day of the experiment, the glass coverslips seeded with the cells were arranged in a home-made fluidic bioreactor, specifically designed to perform targeting experiments (Figure S1A, Supporting Information).[11,20] 15 mL of Vybrant DiO-labeled CDMNVs or CD*MNVs suspension (100 μg mL^{-1}) in complete DMEM without phenol and supplemented with 25×10^{-3} M HEPES were perfused through the bioreactor at a speed of 12 mL min^{-1} for 6 h at 37 °C, by exploiting an Ibidi fluidic device pump (Ibidi). At the end of the experiment, the cells were washed with DPBS and fixed with 4% of paraformaldehyde (PFA) at 4 °C for 20 min, followed by three washes with DPBS. Thereafter, cells were stained with TRITC-phalloidin 0.5% (Sigma Aldrich) and Hoechst 33342 0.1% (Invitrogen) in DPBS for 2 h at 37 °C. The samples were washed three times with DPBS and then imaged with a confocal laser scanning microscope (C2s, Nikon). The semiquantitative analysis of internalization was performed considering the colocalization of the signal of nanovectors (green) and the cells, identified by the cytoskeletal actin labeling (red).

BBB Crossing Experiments: In order to test the BBB crossing abilities of CDMNVs with respect to CD*MNVs, a biomimetic fluidic bioreactor setup in the laboratory was used (Figure S1B, Supporting Information),[11,20,94] composed of a poly(methyl methacrylate) (PMMA) structure with thin poly(dimethyl siloxane) (PDMS) gaskets, forming two compartments. The upper one is a 18 mm × 5 mm channel, where a flow of 12 mL min^{-1} was applied to mimic the shear stress experienced by endothelial cells in brain capillaries (10 dyn cm^{-2}).[95] The lower compartment is a static chamber (1.8 mL in volume) that can allocate a glass coverslip of 1 cm^2. Between the upper channel and the lower static chamber, a porous membrane of poly(ethylene-terephthalate) (PET) with pores of 3 μm was placed. In order to form the in vitro model of the BBB, a co-culture of 5×10^3 cells cm^{-2} of human primary astrocytes (HA, Alphabioregen) and 5×10^3 cells cm^{-2} of human brain vascular pericytes (HBVP, ScienCell) were seeded in the lower side of the PET membrane with a volume of 1.8 mL astrocyte growth medium (Alphabioregen); the surface of the PET membrane was previously treated for 1 h with surface-coating solution (Alphabiocoat, Alphabioregen), following the manufacturer's protocol. 24 h after the HA/HBVP seeding, human brain microvascular endothelial cells (hCMEC/D3, Millipore) were seeded (25×10^4 cell cm^{-2}) on the upper side of the PET membrane, by using 400 μL of EndoGrow (Merk-Millipore). During the following 5 d, culture medium was replaced every day both in the upper and in the lower chamber.

In order to evaluate the BBB crossing abilities of the nanovectors, two types of experimental configuration were used. In the first one, the bottom chamber of the bioreactor was left empty, in order to collect and quantify the nanovectors crossed, avoiding underestimations due to nanovectors uptake by cells. In the second configuration, patient-derived GBM cells were conversely seeded in the bottom chamber, in order to evaluate whether CDMNVs (or CD*MNVs) were still be able to be internalized by cancer cells upon BBB crossing. In the latter case, the day before the perfusion, a glass coverslip previously seeded with 1.5×10^4 cells of patient-derived GBM was placed in the bottom chamber. The day of the experiment, the quality of the BBB was tested with TEER measurement with a volt/ohm meter (Millipore), and the apparent (P_{app}) and endothelial permeability (P_e) coefficient to 70 kDa FITC-dextran (100 μg mL^{-1}, ThermoFisher) were measured following protocols reported in the literature.[96,97]

In both configurations, 15 mL of Vybrant DiO-labeled CDMNV or CD*MNV dispersion (100 μg mL^{-1}) in complete DMEM without phenol red and with 25×10^{-3} M HEPES were perfused in the bioreactors at 12 mL min^{-1} for 3 h at 37 °C. At the end-point, in the BBB bioreactor configuration void of cancer cells cultures the nanovector suspension was replaced with fresh complete medium, and the medium of the bottom chamber was collected at different time points (3, 24, and 48 h) and the fluorescence read with a Victor X3 plate reader (PerkinElmer) at λ_{ex} = 485 nm and λ_{em} = 535 nm. The concentrations of Vybrant DiO-labeled CDMNVs or CD*MNVs were thereafter obtained by using a calibration curve derived by known concentrations of the nanoparticles.

Concerning the bioreactors with patient-derived GBM cells in the bottom chamber, at the end of the 48 h the cells were fixed with PFA 4% at 4 °C for 20 min, and processed for nucleus and f-actin staining, as already described, before observation through confocal microscopy. The signal of the nanoparticles was detected by exploiting their scattering properties (λ_{ex} = 642 nm, λ_{em} = 535 nm), and the analysis of the colocalization cells/nanoparticles was performed using the NIS Elements software (Nikon).

CDMNV Internalization Investigation: 1×10^4 GBM patient-derived cells were seeded in the middle of a WillCo dish with 200 μL of complete medium, and were treated with 100 μg mL^{-1} of CDMNVs the day after seeding, for 6 and 24 h. The cells were fixed and thereafter underwent immunostaining procedure: 10 min of permeabilization with Triton X (1:1000 in DPBS) and equilibration/nucleus staining with Hoechst (1:1000, Invitrogen) were performed in goat serum (GS, Sigma-Aldrich) 10% in DPBS for 30 min at 37 °C. Cells were then incubated with primary anti-clathrin or anti-caveolin-1 rabbit antibody (Abcam, 1:200 dilutions) for 2 h at 37 °C. After three washing steps with GS 10% in DPBS, a TRITC goat anti-rabbit secondary antibody (1:250, Invitrogen) was incubated at 37 °C for 2 h. Confocal acquisitions were performed as previously described, exploiting nanoparticle scattering signal.

CDMNV fate inside cells was also investigated by considering the uptake in lysosomes and in late endosomes. Patient-derived GBM cells, previously seeded in WillCo dishes at a concentration of 10^4 cell cm^{-2}, were incubated for 6, 24, and 96 h with 100 μg mL^{-1} of CDMNVs. The administration time of 24 h represents the time point used in acute stimulation treatments, whereas the 96 h administration is the endpoint of the chronic AMF stimulations (see following sections for further details). At the end of the incubation, the acidotropic fluorescent dye Lysotracker Deep Red (1:2000 dilution, Invitrogen) was added in complete DMEM without phenol red, together with Hoechst 33342 (1:1000 dilution, Invitrogen), before additional 40 min of incubation at 37 °C. Eventually, the staining solution was replaced with 200 μL of complete medium without phenol red supplemented with HEPES 25×10^{-3} M. Confocal acquisitions were performed as previously described. In all cases, the colocalization between CDMNV and organelle signals was assessed using the NIS Elements software (Nikon).

Nanovectors Cytocompatibility: The metabolic activity of cells after treatment with the nanovectors was assessed on patient-derived GBM spheroids, mimicking the possible tumor response. After formation, five

spheroids for each experimental condition were collected and put in 3 mL of complete DMEM in bijoux tubes (ThermoScientific). Based on the experimental results from the drug screenings, regorafenib was selected as the drug to be loaded in the nanovectors (please read relevant section in the Results part). The experimental conditions were thus control (untreated spheroids), spheroids treated with CDMNVs at increasing concentrations (10, 30, 50 100, 150, 300, 500 μg mL^{-1}), spheroids treated with Reg-CDMNVs at increasing concentrations (10, 30, 50 100, 150, 300, 500 μg mL^{-1}), and spheroids treated with free drug at concentrations corresponding to those ones loaded in the Reg-CDMNVs (0.23, 0.68, 1.15, 2.3, 3.4, 6.8, 11.5 × 10^{-6} M). After 24 and 72 h of incubation, the cell culture medium was replaced with 500 μL of WST-1 (Abcam) solution (1:20) in complete DMEM without phenol red; after 1 h of incubation, the absorbance at 450 nm was evaluated with a Victor X3 plate reader (PerkinElmer). The data are indicated as % of metabolic activity with respect to the control.

AMF Treatments: Chronic AMF stimulations were performed by using the same protocol for all the experiments performed in this work. 10^4 cells were seeded in the center of WillCo dishes in 200 μL of complete medium. Eight experimental classes were considered: untreated cells (control), untreated cells exposed to AMF (control + AMF), cells treated with free regorafenib 2.3 × 10^{-6} M, cells treated with free regorafenib 2.3 × 10^{-6} M and exposed to AMF, cells treated with 100 μg mL^{-1} of CDMNVs, cells treated with 100 μg mL^{-1} of CDMNVs and exposed to AMF, cells treated with 100 μg mL^{-1} of Reg-CDMNVs (corresponding to 2.3 × 10^{-6} M of drug), cells treated with 100 μg mL^{-1} of Reg-CDMNVs exposed to AMF. The day after the seeding, the cells were treated by replacing the medium with dispersions in complete medium supplemented with 25 × 10^{-3} M of HEPES in order to maintain the same pH condition during the AMF stimulation. After 24 h of incubation, samples undergoing AMF treatment were subjected to a 2 h d^{-1} 4-d stimulation with a MagneTherm device (NanoTherics), set at an applied magnetic field of 20 mT and a frequency of 97.5 kHz, by using a water-cooled coil of 17 turns and 56 mm (inner diameter), maintained at 37 °C. All the experimental classes not undergoing AMF treatment were left in the incubator throughout the duration of the experiment. For acute stimulation testing, just one AFM treatment after 24 h of incubation was performed.

Investigations on Lysosomal Membrane Permeabilization and Release of Proteolytic Enzymes: The release of proteolytic enzymes after LMP was assessed by immunostaining of cathepsin D. Patient-derived GBM cells were seeded and treated as reported in previous Section. Immediately after the last AMF stimulus, cells were washed with DPBS and fixed with 1 mL of methanol (Sigma-Aldrich) at −20 °C for 5 min. After three washing steps with DPBS, samples were permeabilized with Triton X-100 (1:1000 in DPBS) for 10 min, and thereafter incubated with GS 10% in DPBS for 30 min at 37 °C with Hoechst 33342 (Invitrogen) 1:1000 and TRITC-phalloidin (Sigma-Aldrich) 1:200. Then, cells were incubated with a primary anti-cathepsin D rabbit antibody (GeneTex) 1:300 in GS 10%, for 2 h at 37 °C. After three washing steps with GS 10% in DPBS, a FITC goat anti-rabbit secondary antibody (GoxRa, Invitrogen) 1:250 in GS 10% was incubated for 2 h at 37 °C. Images were acquired with a confocal microscope, as already described.

Induction of Intracellular Stress by Magnetic Hyperthermia: The generation of heat-mediated stress upon magnetic hyperthermia was monitored by assessing the expression of the heat shock protein 70 (HSP70). Patient-derived GBM cells were seeded and treated as previously reported (10^4 cell cm^{-2} in the center of WillCo dishes). A positive control for heat stress was induced by incubating cells at 40 °C for 2 h. 1 h after the end of the acute AMF stimulus, cells were fixed with PFA 4% at 4 °C for 20 min, washed three times with DPBS, permeabilized with Triton x100 (1:1000 in DPBS) for 10 min, and equilibrated for 30 min at 37 °C with 10% GS in DPBS. Cell nuclei were stained with Hoechst 33342 1:1000 and the samples were incubated with anti-HSP70 primary rabbit antibody (GeneTex) 1:300 in GS 10% for 2 h at 37 °C. After three washing steps with GS 10% in DPBS, 400 μL of FITC goat anti-rabbit secondary antibody (Invitrogen) 1:250 was added for a 2 h incubation at 37 °C. Finally, f-actin was stained with TRITC-phalloidin as already described. Confocal microscopy was eventually performed.

The mitochondrial damage related to oxidative stress was studied by evaluating an increase of the expression of the mitochondrial heat shock protein 90 (HSP90), known as TRAP1. Patient-derived GBM cells were seeded and treated according to an acute stimulation, as previously described. Simultaneously, a positive control for oxidative stress was carried out by treating cells with TBH 2.5 × 10^{-3} M for 2 h, without AMF stimulation. 1 h after the end of the acute stimulus, all the samples were washed with DPBS and fixed with 4% PFA at 4 °C for 20 min. Then, the cells were washed with DPBS, equilibrated with 10% GS, and the nuclei were stained with Hoechst 33342 1:1000 for 30 min at 37 °C. Primary rabbit antibody anti-TRAP1 (GeneTex) 1:300 in 10% GS was used for an incubation of 2 h at 37 °C. After three washing steps, FITC goat-anti-rabbit secondary antibody (Invitrogen) 1:250 in GS 10% was incubated for 2 h at 37 °C. Images were acquired with confocal microscopy, as described earlier.

Migration Properties after Magnetic Hyperthermia: Five patient-derived GBM spheroids, obtained as previously reported, were collected in WillCo dishes with 250 μL of complete DMEM supplemented with 25 × 10^{-3} M of HEPES. After 2 d, the medium was replaced according to the chronic treatment previously described (2 h of AMF stimulation for 4 d and eight experimental classes: untreated spheroids -control-, control + AMF, 2.3 × 10^{-6} M of regorafenib, 2.3 × 10^{-6} M of regorafenib + AMF, 100 μg mL^{-1} of CDMNVs, 100 μg mL^{-1} of CDMNVs + AMF, 100 μg mL^{-1} of Reg-CDMNVs (corresponding to 2.3 × 10^{-6} M of drug), 100 μg mL^{-1} of Reg-CDMNVs + AMF). At the beginning and at the end of the experimental protocol, photos of the spheroids were taken by bright-field microscopy and analyzed with the ImageJ software in terms of "migration length," defined as the distance from the border of the spheroid to the furthest cells at the edge of the migration front.

Therapeutic Effects: In order to study the decrease of cell metabolic activity during the AMF chronic stimulation and to identify the end-point of the treatment, WST-1 assay was performed, as already described, after each AFM stimulus for the all duration of the stimulation protocol.

The expression of caspase-8, an apoptosis marker, was evaluated on patient-derived GBM spheroids at the end (1 h later) of the chronic treatment. The samples were washed with DPBS w/o Ca^{2+} and Mg^{2+} (Euroclone), trypsinized (with 150 μL of 0.05% trypsin/EDTA solution for 8 min at 37 °C under gentle pipetting), and obtained cell pellets resuspended in 300 μL of complete medium supplemented with 60 μL of CaspGLOW Fluorescein Active Caspase-8 Staining Kit (Biovision), and maintained 40 min at 37 °C under CO_2 5%. The samples were thereafter centrifuged at 3000 rpm for 6 min, rinsed with washing buffer, and eventually resuspended in 300 μL of the same washing buffer. Analyses were carried out by flow cytometry (Cytoflex, Beckman Coulter) at λ_{ex} = 488 nm and λ_{em} = 525−540 nm.

A "live/dead" assay was also carried out after chronic AMF treatments, performing an incubation of 15 min at 37 °C after the last AFM stimulus with a solution of complete medium without phenol red (Sigma-Aldrich) supplemented with calcein-AM 4 × 10^{-9} M (ThermoFisher scientific), ethidium homodimer-1 4 × 10^{-9} M (Thermoscientific), and Hoechst 33342 20 × 10^{-6} M (Invitrogen). After washing with PBS, images were acquired by confocal microscopy, as described before. The data were indicated as % of dead or live cells with respect to the total number of cells in each sample.

Statistical Analysis: The statistical analysis was performed by one-way ANOVA followed by Bonferroni's correction by using OriginLab Software. Concerning the migration assay, data were analyzed by Kruskal–Wallis ANOVA with OriginLab Software.

Supporting Information

Supporting Information is available from the Wiley Online Library or from the author.

Acknowledgements

D.D.P. and C.P. contributed equally to this work. The research leading to these results has received funding from AIRC under IG 2020 – ID 24454

– P.I. G.C. The authors would like to thank Prof. Federica Barbieri (Università di Genova, Italy) for her advices on primary GBM cell cultures, Mr. Alessio Carmignani (*Istituto Italiano di Tecnologia*, Italy) for technical support, and Dr. Postolache Petronel (University of Iasi, Romania) for VSM measurements.

Open Access Funding provided by Istituto Italiano di Tecnologia within the CRUI-CARE Agreement.

Conflict of Interest

The authors declare no conflict of interest.

Data Availability Statement

The data that support the findings of this study are available from the corresponding author upon reasonable request.

Keywords

glioblastoma, homotypic targeting, magnetic hyperthermia, personalized medicine

Received: December 1, 2022
Revised: March 21, 2023
Published online: May 2, 2023

[1] H. Xu, J. Chen, H. Xu, Z. Qin, *Front. Aging Neurosci.* **2017**, *9*, 1.
[2] A. Degl'Innocenti, N. di Leo, G. Ciofani, *Adv. Ther.* **2020**, *3*, 1900152.
[3] A. D'Alessio, G. Proietti, G. Sica, B. M. Scicchitano, *Cancers* **2019**, *11*, 469.
[4] A. Sabu, T.-I. Liu, ⊥ Siew, S. Ng, R.-A. Doong, Y.-F. Huang, H.-C. Chiu, *ACS Appl. Mater. Interfaces* **2022**, *15*, 158.
[5] W. M. Pardridge, *Pharm. Res.* **2007**, *24*, 1733.
[6] G. Minniti, V. De Sanctis, R. Muni, F. Filippone, A. Bozzao, M. Valeriani, M. F. Osti, U. De Paula, G. Lanzetta, V. Tombolini, R. M. Enrici, *J. Neurooncol.* **2008**, *88*, 97.
[7] C. Fernandes, A. Costa, L. Osorio, R. C. Lago, P. Linhares, B. Carvalho, C. Caerio, *Glioblastoma*, Codon Publications, Brisbane, AU, **2017**, pp. 197–241.
[8] C. Martinelli, C. Pucci, G. Ciofani, *APL Bioeng.* **2019**, *3*, 011502.
[9] A. V. Kroll, R. H. Fang, L. Zhang, *Bioconjugate Chem.* **2017**, *28*, 23.
[10] R. H. Fang, C. M. J. Hu, B. T. Luk, W. Gao, J. A. Copp, Y. Tai, D. E. O'Connor, L. Zhang, *Nano Lett.* **2014**, *14*, 2181.
[11] D. De Pasquale, A. Marino, C. Tapeinos, C. Pucci, S. Rocchiccioli, E. Michelucci, F. Finamore, L. McDonnell, A. Scarpellini, S. Lauciello, M. Prato, A. Larrañaga, F. Drago, G. Ciofani, *Mater. Des.* **2020**, *192*, 108742.
[12] S. M. Wilhelm, J. Dumas, L. Adnane, M. Lynch, C. A. Carter, G. Schütz, K. H. Thierauch, D. Zopf, *Int. J. Cancer* **2011**, *129*, 245.
[13] Stivarga | European Medicines Agency, https://www.ema.europa.eu/en/medicines/human/EPAR/stivarga, (accessed: October 2022).
[14] Regorafenib | FDA, https://www.fda.gov/drugs/resources-information-approved-drugs/regorafenib, (accessed: October 2022).
[15] Agenzia italiana del farmaco commissione consultiva tecnico scientifica, **2019**.
[16] G. Lombardi, G. L. De Salvo, A. A. Brandes, M. Eoli, R. Rudà, M. Faedi, I. Lolli, A. Pace, B. Daniele, F. Pasqualetti, S. Rizzato, L. Bellu, A. Pambuku, M. Farina, G. Magni, S. Indraccolo, M. P. Gardiman, R. Soffietti, V. Zagonel, *Lancet Oncol.* **2019**, *20*, 110.
[17] G. Lombardi, P. Del Bianco, A. A. Brandes, M. Eoli, R. Rudà, T. Ibrahim, I. Lolli, S. Rizzato, B. Daniele, A. Pace, F. Pasqualetti, M. Caccesse, E. Bergo, G. Magni, G. L. De Salvo, V. Zagonel, *Eur. J. Cancer* **2021**, *155*, 179.
[18] G. Lombardi, M. Caccese, M. Padovan, G. Cerretti, G. Pintacuda, R. Manara, F. Di Sarra, V. Zagonel, *Cancers* **2021**, *13*, 4731.
[19] C. Pucci, A. Degl'Innocenti, M. B. Gümüş, G. Ciofani, *Biomater. Sci.* **2022**, *10*, 2103.
[20] C. Pucci, D. De Pasquale, A. Marino, C. Martinelli, S. Lauciello, G. Ciofani, *ACS Appl. Mater. Interfaces* **2020**, *12*, 29037.
[21] P. M. Hallam, M. Gómez-Mingot, D. K. Kampouris, C. E. Banks, *RSC Adv.* **2012**, *2*, 6672.
[22] T. Yamashita, P. Hayes, *Appl. Surf. Sci.* **2008**, *254*, 2441.
[23] R. R. Shah, T. P. Davis, A. L. Glover, D. E. Nikles, C. S. Brazel, *J. Magn. Magn. Mater.* **2015**, *387*, 96.
[24] P. G. Rouxhet, A. M. Misselyn-Bauduin, F. Animou, M. J. Genet, Y. Adriaensen, T. Desille, P. Bodson, C. Deroanne, *Surf. Interface Anal.* **2008**, *40*, 718.
[25] D. Beamson, G. Briggs, *High Resolution XPS of Organic Polymers*, Wiley, Chichester **2022**, 225.
[26] H. Curtis, N. S. Barnes, *Biology*, Worth Publishers, New York **1989**.
[27] R. Hine, *The Facts on File Dictionary of Biology*, Checkmark Books, New York **1999**.
[28] G. M. Cooper, R. E. Hausman, *The Cell: A Molecular Approach*, 2nd ed., **2007**.
[29] R. J. S. Sneath, D. C. Mangham, *Mol. Pathol.* **1998**, *51*, 191.
[30] X. Liu, R. Taftaf, M. Kawaguchi, Y. F. Chang, W. Chen, D. Entenberg, Y. Zhang, L. Gerratana, S. Huang, D. B. Patel, E. Tsui, V. Adorno-Cruz, S. M. Chirieleison, Y. Cao, A. S. Harney, S. Patel, A. Patsialou, Y. Shen, S. Avril, H. L. Gilmore, J. D. Lathia, D. W. Abbott, M. Cristofanilli, J. S. Condeelis, H. Liu, *Cancer Discovery* **2019**, *9*, 96.
[31] M. Kawaguchi, N. Dashzeveg, Y. Cao, Y. Jia, X. Liu, Y. Shen, H. Liu, *J. Biol. Chem.* **2020**, *295*, 2640.
[32] R. R. Kudarha, K. K. Sawant, *Drug Delivery Transl. Res.* **2021**, *11*, 1994.
[33] W. Yu, L. Yang, T. Li, Y. Zhang, *Front. Oncol.* **2019**, *9*, 989.
[34] S. Owczarek, V. Berezin, *Int. J. Biochem. Cell Biol.* **2012**, *44*, 1.
[35] O. Karaagac, H. Köçkar, *J. Magn. Magn. Mater.* **2022**, *551*, 169140.
[36] A. S. Teja, P. Y. Koh, *Prog. Cryst. Growth Charact. Mater.* **2009**, *55*, 22.
[37] A. H. Lu, E. L. Salabas, F. Schüth, *Angew. Chem., Int. Ed.* **2007**, *46*, 1222.
[38] M. Anbarasu, M. Anandan, E. Chinnasamy, V. Gopinath, K. Balamurugan, *Spectrochim. Acta, Part A* **2015**, *135*, 536.
[39] M. F. Tai, C. W. Lai, S. B. Abdul Hamid, *J. Nanomater.* **2016**, *2016*, 1.
[40] P. Deng, Z. Wang, Z. Pan, A.-J. Qin, M. Liu, G. Antarnusa, E. Suharyadi, *Mater. Res. Express* **2020**, *7*, 056103.
[41] V. Patsula, M. Moskvin, S. Dutz, D. Horák, *J. Phys. Chem. Solids* **2016**, *88*, 24.
[42] Q. Li, C. W. Kartikowati, S. Horie, T. Ogi, T. Iwaki, K. Okuyama, *Sci. Rep.* **2017**, *7*, 1.
[43] A. Muela, D. Muñoz, R. Martín-Rodríguez, I. Orue, E. Garaio, A. Abad Díaz De Cerio, J. Alonso, J. Á. García, M. L. Fdez-Gubieda, *J. Phys. Chem. C* **2016**, *120*, 24437.
[44] K. Simeonidis, M. P. Morales, M. Marciello, M. Angelakeris, P. De La Presa, A. Lazaro-Carrillo, A. Tabero, A. Villanueva, O. Chubykalo-Fesenko, D. Serantes, *Sci. Rep.* **2016**, *6*, 1.
[45] B. Herrero de la Parte, I. Rodrigo, J. Gutiérrez-Basoa, S. Iturrizaga Correcher, C. Mar Medina, J. J. Echevarría-Uraga, J. A. Garcia, F. Plazaola, I. García-Alonso, *Cancers* **2022**, *14*, 3084.
[46] Y. Piñeiro-Redondo, M. Bañobre-López, I. Pardiñas-Blanco, G. Goya, M. A. López-Quintela, J. Rivas, *Nanoscale Res. Lett.* **2011**, *6*, 383.
[47] N. Yang, W. Xiao, X. Song, W. Wang, X. Dong, *Nano-Micro Lett.* **2020**, *12*, 1.
[48] J. P. Fisher, D. C. Adamson, *Biomedicines* **2021**, *9*, 324.

[49] FDA, Cder, *Rx Only BiCNU (Carmustine for Injection)*, https://www.accessdata.fda.gov/drugsatfda_docs/label/2013/017422s046lbl.pdf, (accessed: October 2022).
[50] FDA, GLIADEL WAFER (carmustine implant), for intracranial use, www.fda.gov/medwatch, (accessed: October 2022).
[51] P. Chène, *Nat. Rev. Cancer* **2003**, *3*, 102.
[52] R. Villalonga-Planells, L. Coll-Mulet, F. Martínez-Soler, E. Castaño, J. J. Acebes, P. Giménez-Bonafé, J. Gil, A. Tortosa, *PLoS One* **2011**, *6*, e18588.
[53] C. F. Guo, Y. Zhuang, Y. Chen, S. Chen, H. Peng, S. Zhou, *Biomark. Med.* **2020**, *14*, 1139.
[54] S. Y. Lee, *Genes Dis.* **2016**, *3*, 198.
[55] L. Abou-Elkacem, S. Arns, G. Brix, F. Gremse, D. Zopf, F. Kiessling, W. Lederle, *Mol. Cancer Ther.* **2013**, *12*, 1322.
[56] Y. S. Chang, J. Adnane, P. A. Trail, J. Levy, A. Henderson, D. Xue, E. Bortolon, M. Ichetovkin, C. Chen, A. McNabola, D. Wilkie, C. A. Carter, I. C. A. Taylor, M. Lynch, S. Wilhelm, *Cancer Chemother. Pharmacol.* **2007**, *59*, 561.
[57] Nexavar (sorafenib) FDA Approval History – Drugs.com, https://www.drugs.com/history/nexavar.html, (accessed: October 2022).
[58] S. Fredenberg, M. Wahlgren, M. Reslow, A. Axelsson, *Int. J. Pharm.* **2011**, *415*, 34.
[59] R. H. Fang, A. V. Kroll, W. Gao, L. Zhang, *Adv. Mater.* **2018**, *30*, 1.
[60] H. C. Helms, N. J. Abbott, M. Burek, R. Cecchelli, P. O. Couraud, M. A. Deli, C. Förster, H. J. Galla, I. A. Romero, E. V. Shusta, M. J. Stebbins, E. Vandenhaute, B. Weksler, B. Brodin, *J. Cereb. Blood Flow Metab.* **2015**, *36*, 862.
[61] C. Rampon, N. Weiss, C. Deboux, N. Chaverot, F. Miller, D. Buchet, H. Tricoire-Leignel, S. Cazaubon, A. Baron-Van Evercooren, P.-O. Couraud, *Stem Cells* **2008**, *26*, 1673.
[62] M. Díaz-Coránguez, J. Segovia, A. López-Ornelas, H. Puerta-Guardo, J. Ludert, B. Chávez, N. Meraz-Cruz, L. González-Mariscal, *PLoS One* **2013**, *8*, e60655.
[63] F. R. Brennan, J. K. O'Neill, S. J. Allen, C. Butter, G. Nuki, D. Baker, *Immunology* **1999**, *98*, 427.
[64] S. J. H. Soenen, N. Nuytten, S. F. De Meyer, S. C. De Smedt, M. De Cuyper, *Small* **2010**, *6*, 832.
[65] F. Shen, J. K. Park, *Anal. Chem.* **2018**, *90*, 920.
[66] E. Cazares-Cortes, S. Cabana, C. Boitard, E. Nehlig, N. Griffete, J. Fresnais, C. Wilhelm, A. Abou-Hassan, C. Ménager, *Adv. Drug Delivery Rev.* **2019**, *138*, 233.
[67] P. Boya, G. Kroemer, *Oncogene* **2008**, *27*, 6434.
[68] F. Wang, R. Gómez-Sintes, P. Boya, *Traffic* **2018**, *19*, 918.
[69] T. Kallunki, O. D. Olsen, M. Jäättelä, *Oncogene* **2013**, *32*, 1995.
[70] M. Moros, A. Ambrosone, G. Stepien, F. Fabozzi, V. Marchesano, A. Castaldi, A. Tino, J. M. De La Fuente, C. Tortiglione, *Nanomedicine* **2015**, *10*, 2167.
[71] A. Riedinger, P. Guardia, A. Curcio, M. A. Garcia, R. Cingolani, L. Manna, T. Pellegrino, *Nano Lett.* **2013**, *13*, 2399.
[72] M. Tavaria, T. Gabriele, I. Kola, R. L. Anderson, *Cell Stress Chaperones* **1996**, *1*, 23.
[73] R. Rosenzweig, N. B. Nillegoda, M. P. Mayer, B. Bukau, *Nat. Rev. Mol. Cell Biol.* **2019**, *20*, 665.
[74] E. A. Craig, *BMC Biol.* **2018**, *16*, 11.
[75] I. Masgras, C. Sanchez-Martin, G. Colombo, A. Rasola, *Front. Oncol.* **2017**, *7*, 1.
[76] G. Hua, Q. Zhang, Z. Fan, *J. Biol. Chem.* **2007**, *282*, 20553.
[77] M. Mesárošová, K. Kozics, A. Bábelová, E. Regendová, M. Pastorek, D. Vnuková, B. Buliaková, F. Rázga, A. Gábelová, *Toxicol. Lett.* **2014**, *226*, 303.
[78] G. Huang, H. Chen, Y. Dong, X. Luo, H. Yu, Z. Moore, E. A. Bey, D. A. Boothman, J. Gao, *Theranostics* **2013**, *3*, 116.
[79] K. Bedard, K. H. Krause, *Physiol. Rev.* **2007**, *87*, 245.
[80] A. Sola-Leyva, Y. Jabalera, M. A. Chico-Lozano, M. P. Carrasco-Jiménez, G. R. Iglesias, C. Jimenez-Lopez, *J. Mater. Chem. B* **2020**, *8*, 7667.
[81] R. Gupta, D. Sharma, *ACS Appl. Nano Mater.* **2020**, *3*, 2026.
[82] R. Gupta, D. Sharma, *Colloids Surf., B* **2021**, *205*, 111870.
[83] J. A. Zazo, G. Pliego, S. Blasco, J. A. Casas, J. J. Rodriguez, *Ind. Eng. Chem. Res.* **2011**, *50*, 866.
[84] E. Cazares-Cortes, S. Cabana, C. Boitard, E. Nehlig, N. Griffete, J. Fresnais, C. Wilhelm, A. Abou-Hassan, C. Ménager, *Adv. Drug Delivery Rev.* **2019**, *138*, 233.
[85] V. Massey, K. E. Wallner, *Int. J. Radiat. Oncol. Biol. Phys.* **1990**, *18*, 395.
[86] H. Zahreddine, K. L. B. Borden, *Front. Pharmacol.* **2013**, *4*, 1.
[87] C. Pop, P. Fitzgerald, D. R. Green, G. S. Salvesen, *Biochemistry* **2007**, *46*, 4398.
[88] B. Zhong, M. Liu, C. Bai, Y. Ruan, Y. Wang, L. Qiu, Y. Hong, X. Wang, L. Li, B. Li, *Mol. Ther.* **2020**, *28*, 1078.
[89] I. Verbrugge, R. W. Johnstone, M. J. Smyth, *Cell* **2010**, *143*, 1192.
[90] L. Beola, L. Asín, C. Roma-Rodrigues, Y. Fernandez-Afonso, R. M. Fratila, D. Serantes, S. Ruta, R. W. Chantrell, A. R. Fernandes, P. V. Baptista, J. M. de la Fuente, V. Grazú, L. Gutiérrez, *ACS Appl. Mater. Interfaces* **2020**, *12*, 43474.
[91] L. M. Bronstein, X. Huang, J. Retrum, A. Schmucker, M. Pink, B. D. Stein, B. Dragnea, *Chem. Mater.* **2007**, *19*, 3624.
[92] N. Fairley, V. Fernandez, M. Richard-Plouet, C. Guillot-Deudon, J. Walton, E. Smith, D. Flahaut, M. Greiner, M. Biesinger, S. Tougaard, D. Morgan, J. Baltrusaitis, *Appl. Surf. Sci. Adv.* **2021**, *5*, 100112.
[93] R. R. Wildeboer, P. Southern, Q. A. Pankhurst, *J. Phys. D: Appl. Phys.* **2014**, *47*, 495003.
[94] C. Pucci, A. Marino, Ö. Şen, D. De Pasquale, M. Bartolucci, N. Iturrioz-Rodríguez, N. di Leo, G. de Vito, D. Debellis, A. Petretto, G. Ciofani, *Acta Biomater.* **2022**, *139*, 218.
[95] A. D. Wong, M. Ye, A. F. Levy, J. D. Rothstein, D. E. Bergles, P. C. Searson, *Front. Neuroeng.* **2013**, *6*, 1.
[96] A. Siflinger-Birnboim, P. J. del Vecchio, J. A. Cooper, F. A. Blumenstock, J. M. Shepard, A. B. Malik, *J. Cell. Physiol.* **1987**, *132*, 111.
[97] M. Heymans, E. Sevin, F. Gosselet, S. Lundquist, M. Culot, *Eur. J. Pharm. Biopharm.* **2018**, *127*, 453.